DISEASES AND DISORDERS

Adseverin, an actin-binding protein, modulates hypertrophic chondrocyte differentiation and osteoarthritis progression

Byron Chan[1,2], Michael Glogauer[3], Yongqiang Wang[3], Jeffrey Wrana[1], Kin Chan[1], Frank Beier[4], Supinder Bali[4], Boris Hinz[3,5], Justin Parreno[6], Sajjad Ashraf[1], Rita Kandel[1,2]*

In osteoarthritis (OA), a disease characterized by progressive articular cartilage degradation and calcification, the articular chondrocyte phenotype changes and this correlates with actin cytoskeleton alterations suggesting that it regulates gene expression essential for proper phenotype. This study reports that OA is associated with the loss of adseverin, an actin capping and severing protein. Adseverin deletion (Adseverin$^{-/-}$) in mice compromised articular chondrocyte function, by reducing F-actin and aggrecan expression and increasing apoptosis, Indian hedgehog, Runx2, MMP13, and collagen type X expression, and cell proliferation. This led to stiffer cartilage and decreased hyaline and increased calcified cartilage thickness. Together, these changes predisposed the articular cartilage to enhanced OA severity in Adseverin$^{-/-}$ mice who underwent surgical induction of OA. Adseverin$^{-/-}$ chondrocyte RNA sequencing and in vitro studies together suggests that adseverin modulates cell viability and prevents mineralization. Thus, adseverin maintains articular chondrocyte phenotype and cartilage tissue homeostasis by preventing progression to hypertrophic differentiation in vivo. Adseverin may be chondroprotective and a potential therapeutic target.

INTRODUCTION

Articular cartilage is a specialized connective tissue that covers the ends of the bone and is responsible for the pain-free, smooth articulation of synovial joints. Tissue health and function are largely dependent on chondrocyte phenotype stability. Healthy chondrocytes are fine-tuned to balance between anabolic and catabolic functions to maintain the extracellular matrix (ECM) (*1*). In osteoarthritis (OA), however, a disease characterized by progressive degradation of the cartilage matrix, the articular chondrocyte phenotype is lost. Pro-inflammatory cytokines interleukin-1β (IL-1β) and tumor necrosis factor–α (TNF-α) have been implicated as mediators in OA pathogenesis and shown to induce articular chondrocyte dedifferentiation (*2*), proliferation, and apoptosis (*3*), which are features of OA chondrocytes (*2*). Increased chondrocyte apoptosis is also associated with OA pathogenesis as the articular cartilage becomes hypocellular during the later stages of OA (*4*). Furthermore, OA chondrocytes reduce the expression of chondrogenic matrix molecules such as aggrecan and collagen type II while increasing the expression of fibroblastic molecules collagen type I and alpha-smooth muscle actin (αSMA) (*2*, *5*). There can also be evidence of chondrocyte hypertrophy (*1*, *6*, *7*). Although expression of hypertrophic characteristics is a necessary stage in terminal differentiation in the growth plate, when dysregulated in articular cartilage as occurs in OA, it can lead to abnormal matrix remodeling and mineralization that further exacerbates cartilage damage. The acquisition of these changes in phenotype contributes to OA pathogenesis.

The actin cytoskeleton, specifically the depolymerization of filamentous actin (F-actin), has been correlated with the expression of genes that are favorable for the articular chondrocyte phenotype (*8*–*10*), but the underlying mechanism(s) regulating this is not completely known. As actin-binding proteins are responsible for modulating the actin cytoskeleton status through promoting polymerization and depolymerization of actin filaments, this could be one regulatory mechanism. In contrast to healthy articular chondrocytes, OA chondrocytes exhibit a disorganized actin cytoskeleton (*8*) and differentially express actin-binding proteins that lead to actin polymerization (*11*, *12*). Little is known about the role of actin-binding proteins in relation to chondrocyte phenotype, but studies have shown that they are critical for OA progression, articular cartilage development, and homeostasis (*8*). One of these may be adseverin, an actin severing and capping protein, as it has been demonstrated to contribute to the regulation of the articular chondrocyte phenotype through modulation of the actin cytoskeleton in vitro (*13*). However, it is still unclear whether adseverin functions similarly to regulate articular chondrocyte phenotype in vivo and how it influences tissue homeostasis and OA progression.

In this study, we hypothesized that adseverin expression plays a role in maintaining chondrocyte phenotype and its dysregulation leads to cartilage matrix changes which will enhance the progression of OA. We report that adseverin loss in the articular cartilage compromises chondrocyte viability and function to influence the ECM composition and, thus, the mechanical properties of the cartilage. We identify that adseverin deletion resulted in the up-regulation of hypertrophy and proliferation markers such as Indian hedgehog (Ihh), runt-related transcription factor 2 (Runx2), collagen type X, matrix metallopeptidase 13 (MMP13), and Ki67 and is associated with enhanced mineralization potential when cells are treated with inorganic phosphate. These changes disrupt tissue homeostasis as the total articular cartilage thickness decreased over time and ultimately predisposed the tissue to enhanced cartilage

[1]Lunenfeld-Tanenbaum Research Institute, Toronto, ON, Canada. [2]Laboratory Medicine and Pathobiology, University of Toronto, Toronto, ON, Canada. [3]Faculty of Dentistry, University of Toronto, Toronto, ON, Canada. [4]Department of Physiology and Pharmacology, Western University, London, ON, Canada. [5]Laboratory of Tissue Repair and Regeneration, Keenan Research Centre for Biomedical Science of the St. Michael's Hospital, Toronto, ON, Canada. [6]Department of Biological Sciences, University of Delaware, Newark, DE, USA.
*Corresponding author. Email: rita.kandel@sinaihealth.ca

degradation during OA. Thus, adseverin is critical for the regulation of the articular chondrocyte phenotype and articular cartilage homeostasis. Some of these changes are different than those that occur in the postnatal growth plate as adseverin deletion in these chondrocytes appears to decrease hypertrophic differentiation. In growth plate chondrocytes, we observed evidence of growth plate thinning and decreased expression of hypertrophic markers Runx2, collagen type X, and MMP13 following adseverin deletion. This was also associated with decreased cellularity and Ki67 expression and increased apoptosis. Our findings demonstrate that the two cell types respond differently to adseverin loss.

RESULTS

Adseverin expression is down-regulated with IL-1β treatment and OA

IL-1β and TNF-α have been implicated as key mediators in OA pathogenesis (*14*, *15*) so the effects of these cytokines on adseverin expression were examined in primary bovine articular chondrocytes. Quantitative polymerase chain reaction (qPCR) revealed that IL-1β treatment resulted in a significant decrease in adseverin, SRY-box transcription factor 9 (Sox9), collagen type I and II, and aggrecan gene expression. In addition, it also resulted in a significant increase in MMP13 gene expression (Fig. 1A). TNF-α treatment only resulted in a significant decrease in collagen type I and II, aggrecan gene expression, and a significant increase in MMP13 gene expression (Fig. 1B). There was no change in adseverin expression, thus adseverin was mediated by IL-1β and not TNF-α. A combination of both IL-1β and TNF-α treatment did not enhance the effect observed by IL-1β treatment alone (Fig. 1C). Western blot analysis confirmed that adseverin protein expression was significantly decreased by IL-1β after 7 days (Fig. 1D).

As exposure to pro-inflammatory cytokines alone does not fully represent OA, 10-week-old mice underwent surgically induced OA by destabilization of the medial meniscus (DMM) to further examine the relationship between adseverin and OA (Fig. 1E). As expected, histological assessment and Osteoarthritis Research Society International (OARSI) grading of mice at 4 weeks after injury confirmed hyaline cartilage degeneration in the medial femoral condyle (MFC) and tibial plateau (MTP) of DMM compared to sham-operated mice. The articular cartilage of the lateral femoral condyle (LFC) and tibial plateau (LTP) is intact with no signs of damage (Fig. 1, F and G, and fig. S1A). Chondrocyte apoptosis, a hallmark of OA (*16*, *17*), was present in DMM mice as terminal deoxynucleotidyl transferase–mediated deoxyuridine triphosphate nick end labeling (TUNEL) staining revealed a significantly increased number of apoptotic cells in the MFC, MTP, and LFC compared to control mice. Concomitantly phalloidin staining demonstrated a loss of F-actin in the chondrocytes of the MFC and MTP (Fig. 1, H and I, and fig. S1B). Immunohistochemical analysis showed that adseverin expression was significantly decreased not only in the articular cartilage of the MFC and MTP but also in all compartments of the knee joint of DMM versus sham-operated mice (Fig. 1, J and K, and fig. S1C). This decreased adseverin expression was not an artifact of tissue processing as immunoreactivity was observed in growth plate chondrocytes.

At 8 weeks after injury, histology and OARSI scores confirm further cartilage damage indicated by fibrillation, erosion, and osteophyte formation localized to the MFC and MTP of DMM versus sham-operated mice. The cartilage of the lateral compartment remained intact with no signs of damage (fig. S2, A and B). However, similar to the 4-week time point, the TUNEL assay shows a significantly increased number of dead chondrocytes in the MFC and MTP of DMM versus sham-operated mice. Both adseverin and F-actin were lost or significantly reduced in the articular chondrocytes of all compartments of the knee joint compared to sham-operated mice (fig. S2, C to F).

Deletion of adseverin leads to rapid increase in apoptosis and decrease in F-actin in articular chondrocytes before articular cartilage changes

To directly assess the contribution of adseverin to regulating chondrocyte phenotype, an inducible adseverin knockout mouse model driven by CreERT2 expression under the control of the aggrecan promoter was created. Adseverin deletion was induced by tamoxifen administration at 8 weeks of age (Fig. 2A). At 10 weeks, the genotype of the control (Adseverin$^{+/+}$) and knockout (Adseverin$^{-/-}$) mice (Fig. 2B) and the tamoxifen-induced adseverin deletion product was confirmed by PCR (Fig. 2C). Adseverin deletion was confirmed by immunohistochemical staining, which revealed no adseverin in the articular cartilage and postnatal growth plate (Fig. 2D).

The articular cartilage was evaluated for OA changes at 10 weeks of age, which was 9 days after the last tamoxifen dose. Given cartilage changes developed by 4 weeks after DMM (Fig. 1, F and G, and fig. S1A), this time point allowed for the assessment of early changes before these cartilage changes. Histological assessment revealed no significant difference in the cartilage appearance of Adseverin$^{-/-}$ versus Adseverin$^{+/+}$ mice (Fig. 2E). To further characterize cartilage, the total and hyaline and calcified portions of the cartilage thickness were measured (Fig. 2F). No significant differences in these were observed in the knee joint between Adseverin$^{-/-}$ and Adseverin$^{+/+}$ mice (Fig. 2, G to I). However, TUNEL analysis revealed that adseverin deletion resulted in a significant increase in the number of apoptotic cells and there appeared to be a reduction in F-actin in chondrocytes in the mid/deep zone compared to Adseverin$^{+/+}$ mice (Fig. 2, J and K).

Adseverin deletion alters chondrocyte phenotype and increases articular cartilage stiffness

To identify the gene changes due to adseverin deletion, RNA sequencing (RNA-seq) analysis was performed on chondrocytes harvested from native articular cartilage of 10-week-old Adseverin$^{-/-}$ and Adseverin$^{+/+}$ mice. Differential expression analysis revealed a total of 120 significant differentially expressed genes (DEGs), comprising 62 up-regulated (fig. S3A) and 58 down-regulated DEGs (fig. S3B). Of these DEGs, up-regulated genes include Ihh, hedgehog-interacting protein (Hhip), protein patched homolog 1 (Ptch1), and markers of proliferation Ki67, cell division cycle 6 (Cdc6), and cyclin E1 (Ccne1). Whereas down-regulated genes included aggrecan (Acan), a disintegrin and metalloproteinase with thrombospondin motifs 4 (Adamts4), and growth arrest specific 1 (Gas1) (Fig. 3A). Gene set enrichment analysis revealed significantly up-regulated pathways associated with Ihh signaling, cell cycle, and proliferation and significantly down-regulated pathways associated with actin cytoskeleton organization (Fig. 3B). When comparing the average expression of Ihh signaling pathway genes such as Ihh, Hhip, Ptch1, Gli1, and Gli3, majority of these genes were

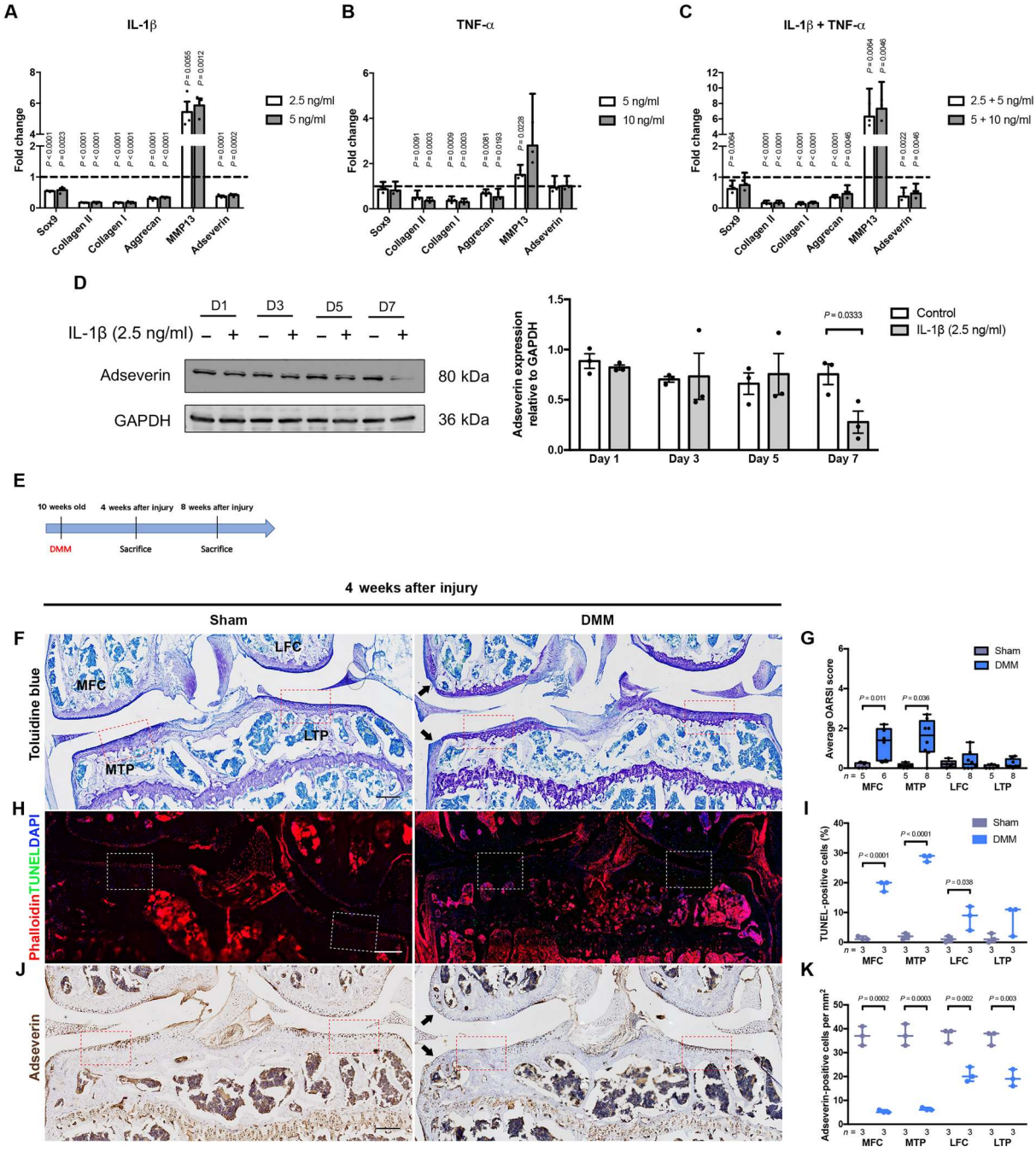

Fig. 1. Adseverin expression is down-regulated with IL-1β exposure in vitro and in a mouse model of OA. Gene expression of primary bovine articular chondrocytes treated with (**A**) IL-1β, (**B**) TNF-α, and (**C**) a combination of both IL-1β and TNF-α. The dashed line represents the gene expression of the control vehicle-treated chondrocytes. *P* values reflect the comparison of the treatment versus control. (**D**) Western blot and densitometry analysis of adseverin protein expression following IL-1β treatment. Results are expressed as means ± SEM of $n = 3$ independent experiments. GAPDH, glyceraldehyde-3-phosphate dehydrogenase. (**E**) Experimental schematic showing the destabilization of the medial meniscus (DMM) timeline. OA severity was determined at 4 weeks by (**F**) histological assessment of toluidine blue–stained coronal sections of the mouse knee joint. MFC, medial femoral condyle; MTP, medial tibial plateau; LFC, lateral femoral condyle; LTP, lateral tibial plateau. The black arrow indicates osteophyte formation. Scale bar, 200 μm. (**G**) Mean Osteoarthritis Research Society International (OARSI) scores. (**H**) Fluorescent images of apoptotic chondrocytes and actin cytoskeleton following staining with terminal deoxynucleotidyl transferase–mediated deoxyuridine triphosphate nick end labeling (TUNEL) (green) and phalloidin (red), respectively. 4′,6-Diamidino-2-phenylindole (DAPI) (blue) stains nuclei. Scale bar, 400 μm. (**I**) Quantification of TUNEL-positive cells in the articular cartilage of all knee compartments following sham or DMM surgery. (**J**) Immunohistochemical staining and (**K**) quantification of adseverin-positive cells in the articular cartilage following sham or DMM surgery. Scale bar, 200 μm. Higher-magnification images of the red or white dashed box in regions are shown in fig. S1. Box plots represent median values and interquartile ranges, and whiskers are plotted using the Tukey method. Dot plots represent the mean with minimum and maximum values. Statistical analysis was assessed using one-way analysis of variance (ANOVA) followed by Dunnett's test for multiple comparisons (A to C) and Student's unpaired two-tailed *t* test (D, G, I, and K). The number of biological replicates in each group and *P* values are indicated in the figure.

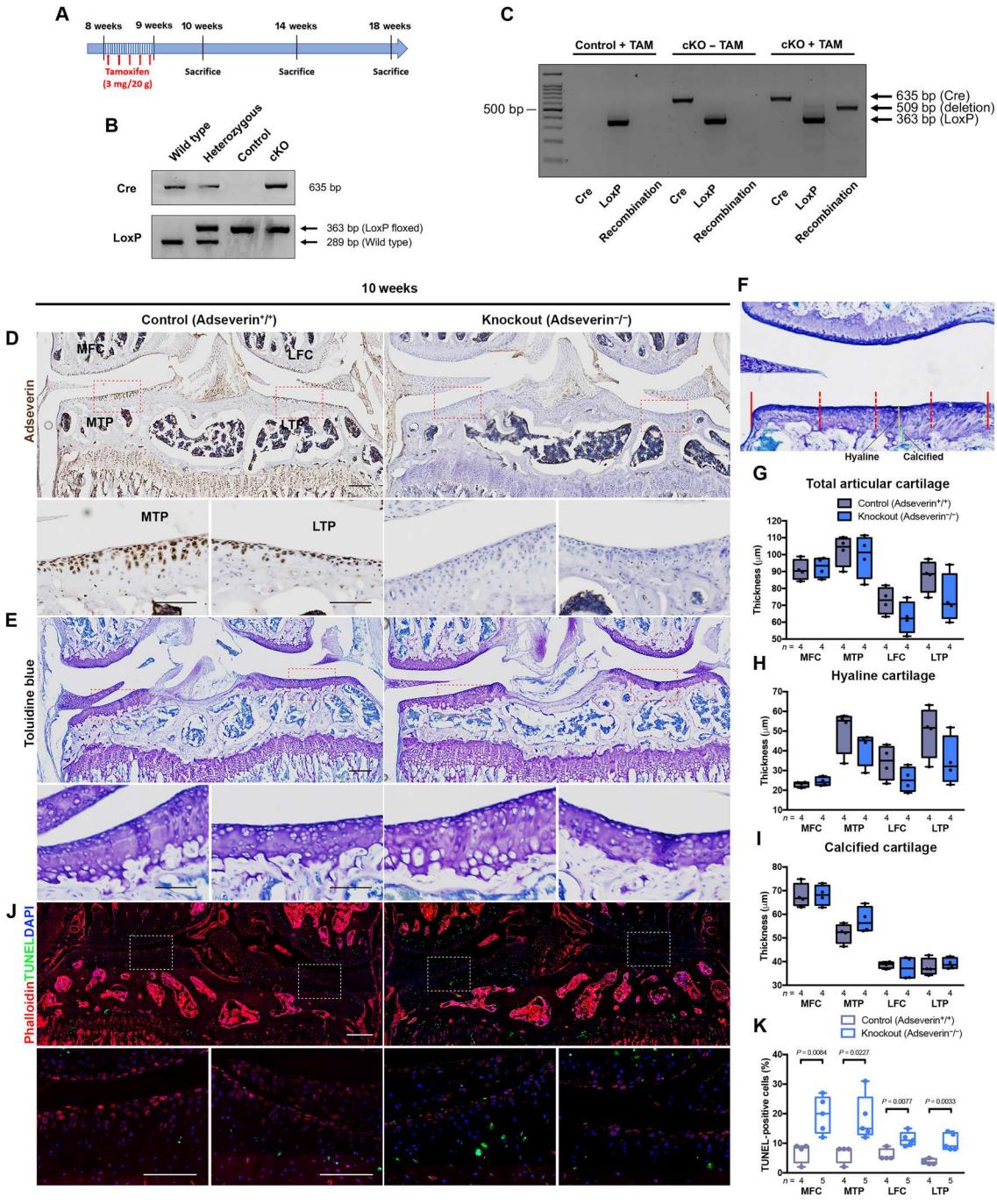

Fig. 2. Deletion of adseverin induces an increase in apoptosis and a decrease in F-actin before articular cartilage changes. (**A**) Schematic of tamoxifen-induced adseverin deletion. (**B**) Genotyping by PCR to confirm the Cre recombinase and homozygous floxed adseverin product, followed by the (**C**) detection of tamoxifen-induced adseverin deletion product. TAM, tamoxifen. At 10 weeks, (**D**) adseverin deletion was confirmed by immunohistochemistry of the articular cartilage of all knee compartments. The bottom photomicrograph shows higher-magnification images of the indicated regions. Scale bars, 200 μm (lower magnification) and 100 μm (higher magnification). (**E**) Toluidine blue–stained coronal sections of the knee joint after tamoxifen-induced adseverin deletion. The bottom photomicrograph shows higher-magnification images of the indicated regions. Scale bar, 200 μm (lower magnification) and 100 μm (higher magnification). (**F**) Toluidine blue–stained section of MTP articular cartilage indicating the hyaline (yellow line) and calcified (green line) cartilage regions. Red dashed lines indicate the approximate locations (quartiles 1/2/3 of the surface of the entire articular cartilage) at which measurements of articular cartilage thickness were taken. (**G**) Mean total articular, (**H**) hyaline, and (**I**) calcified cartilage thickness measurements following adseverin deletion. (**J**) Apoptotic chondrocytes and the actin cytoskeleton were detected by immunofluorescent staining with TUNEL (green) and phalloidin (red), respectively. DAPI (blue) stains nuclei. The bottom photomicrograph shows higher-magnification images of the indicated regions. Scale bars, 400 μm (lower magnification) and 200 μm (higher magnification). (**K**) Quantification of TUNEL-positive cells after adseverin deletion. Box plots represent median values and interquartile ranges, and whiskers are plotted using the Tukey method. Statistical analysis was assessed using Student's unpaired two-tailed *t* test (G to I and K). The number of biological replicates in each group and *P* values are indicated in the figure. Experiments were repeated three times (D) with similar results.

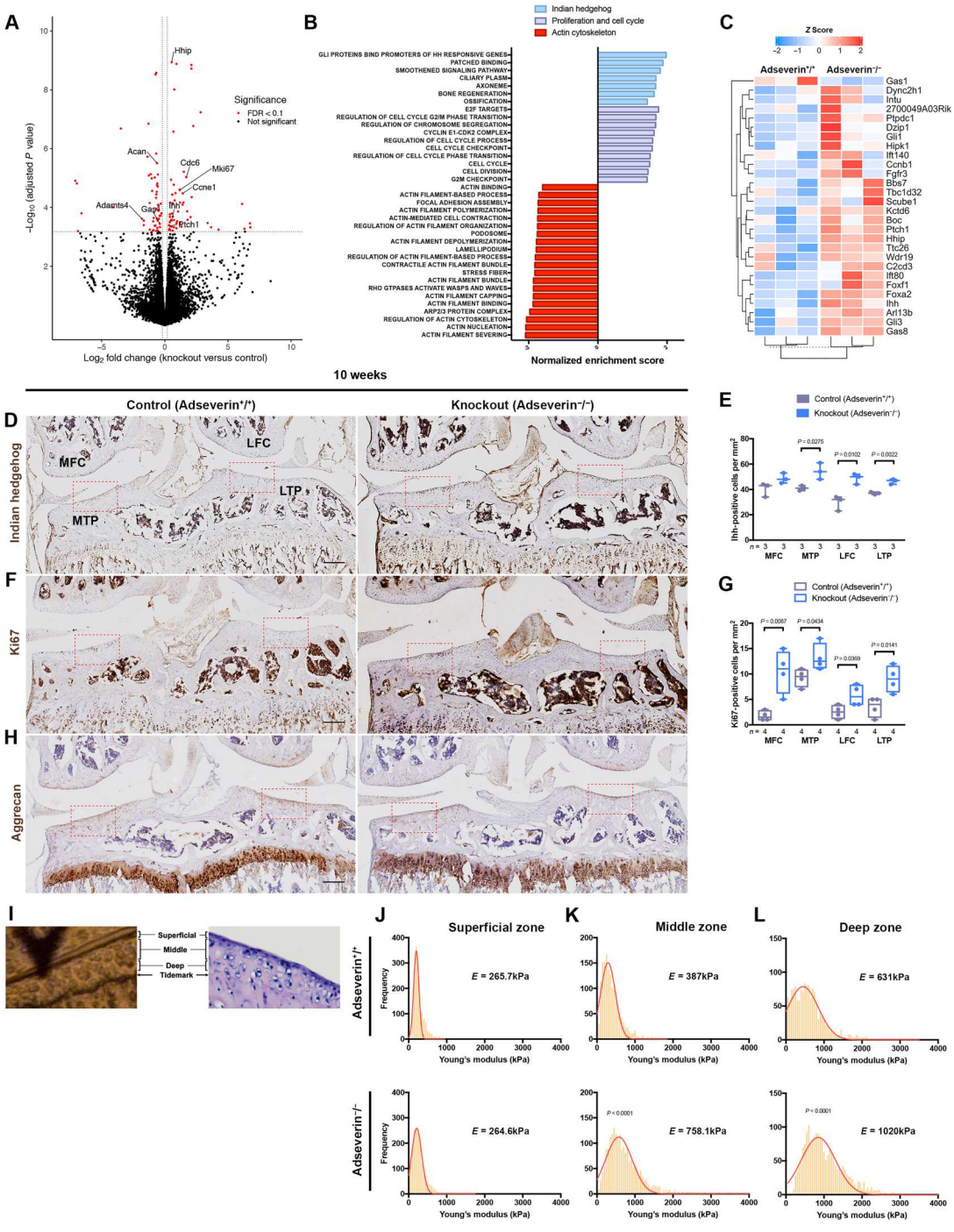

Fig. 3. Adseverin deletion alters the transcriptional profile of articular chondrocytes and leads to increased cartilage stiffness. (**A**) Volcano plot of DEGs from RNA-seq of Adseverin$^{-/-}$ versus Adseverin$^{+/+}$ articular chondrocytes isolated from 10-week-old mice. DEGs indicated by red dot plots are considered significant by false discovery rate (FDR) < 0.1 and $|\log_2$ fold change$| \geq 0.2$. (**B**) Gene set enrichment analysis and functional grouping of up-regulated and down-regulated gene sets, indicated by normalized enrichment scores, in Adseverin$^{-/-}$ compared to Adseverin$^{+/+}$ articular chondrocytes. (**C**) Heatmap expression of Ihh signaling pathway genes. At 10 weeks, immunohistochemical analyses of (**D** and **E**) Ihh, (**F** and **G**) Ki67, and (**H**) aggrecan in the articular cartilage comparing Adseverin$^{-/-}$ and Adseverin$^{+/+}$ mice. Scale bars, 200 μm. Higher-magnification images of the red dashed box regions are in fig. S4. (**I**) Bright-field and hematoxylin and eosin (H&E)–stained images of articular cartilage highlighting the zones assessed by Indentation-type atomic force microscopy (IT-AFM) (×20 magnification). The AFM cantilever is also shown in the bright-field image. Histograms of Young's modulus distribution determined by IT-AFM in the (**J**) superficial, (**K**) middle, and (**L**) deep zone articular cartilage at MTP comparing Adseverin$^{-/-}$ and Adseverin$^{+/+}$ mice. On each histogram, the solid line represents the fitting of the Gaussian distribution. E represents the mean Young's modulus of $n = 3$ mice per genotype, and P values reflect comparisons of the Adseverin$^{-/-}$ versus Adseverin$^{+/+}$ mice. Dot plots represent the mean with minimum and maximum values. Box plots represent median values and interquartile ranges, and whiskers are plotted using the Tukey method. Statistical analysis was assessed using Student's unpaired two-tailed t test (E, G, J, K, and L). The number of biological replicates in each group and P values are indicated in the figure.

highly expressed with adseverin deletion (Fig. 3C). Selected genes identified by RNA-seq results were validated by immunohistochemical staining of 10-week-old Adseverin$^{-/-}$ and Adseverin$^{+/+}$ mouse knee joint sections. Ihh (Fig. 3, D and E, and fig. S4A) and Ki67 (Fig. 3, F and G, and fig. S4B) were significantly up-regulated in the Adseverin$^{-/-}$ versus Adseverin$^{+/+}$ mice. Furthermore, aggrecan staining was decreased markedly in the articular cartilage of Adseverin$^{-/-}$ mice (Fig. 3H and fig. S4C).

Loss of proteoglycans, specifically aggrecan, can result in alterations in the biomechanical properties of the tissue and may contribute to the onset of OA (*18*–*20*). To assess whether this was occurring with adseverin deletion, indentation-type atomic force microscopy (IT-AFM) was used to measure the Young's modulus

as an assessment of stiffness in the depth-dependent articular cartilage zones of 10-week-old mice (Fig. 3I). In the superficial zone, Adseverin$^{-/-}$ and Adseverin$^{+/+}$ showed comparable stiffness indicated by no significant difference in the mean Young's modulus (Fig. 3J). With respect to the middle and deep zones, Adseverin$^{-/-}$ (middle: E = 758.1 kPa, deep: E = 1020 kPa) showed significantly increased mean Young's modulus versus Adseverin$^{+/+}$ (middle: E = 387 kPa, deep: E = 631 kPa) mice (Fig. 3, K and L). These results indicate that adseverin loss leads to stiffening of articular cartilage.

Loss of adseverin leads to progressive thinning of the hyaline cartilage

Although there were no discernable differences in the macroscopic and histologic appearance of the articular cartilage between Adseverin$^{-/-}$ and Adseverin$^{+/+}$ mice at 10 weeks, it was postulated that additional time was needed for structural changes to manifest. For this reason, cartilage thickness was measured at 14 and 18 weeks. By 18 weeks (Fig. 4), there were significant decreases in total cartilage thickness due to the thinning of the hyaline component of the cartilage (Fig. 4, E to G) in all compartments of the knee in the Adseverin$^{-/-}$ compared to Adseverin$^{+/+}$ mice. This loss of hyaline cartilage thickness was evident at the earlier 14-week time point (Fig. 4, A and C) but did not result in significant changes in total cartilage thickness in the medial compartment (Fig. 4B) likely due to the variability between animals. The calcified cartilage thickness was not significantly different at 14 weeks (Fig. 4D) but was significantly increased in the LTP at 18 weeks (Fig. 4H) between Adseverin$^{-/-}$ and Adseverin$^{+/+}$ mice. These findings suggest that the effects of adseverin deletion disrupt the maintenance of the ECM and lead to the progressive thinning of the articular cartilage.

Adseverin deletion promotes hypertrophy in the articular cartilage

To investigate whether the decrease in the hyaline cartilage thickness was correlated to the phenotypic changes induced by adseverin loss, immunohistochemical analyses were performed on Adseverin$^{-/-}$ and Adseverin$^{+/+}$ mice at 14 and 18 weeks. At 14 weeks, adseverin expression remains significantly decreased in the articular cartilage of Adseverin$^{-/-}$ versus Adseverin$^{+/+}$ mice (Fig. 5, A and B, and fig. S5A). Consistent with findings of the 10-week time point, Ihh (Fig. 5, C and D, and fig. S5B), Ki67 (Fig. 5, E and F, and fig. S5C), and apoptosis (Fig. 5, H and I, and fig. S5E) remain significantly increased in Adseverin$^{-/-}$ versus Adseverin$^{+/+}$ mice. There was decreased staining for aggrecan in the mid/deep zone cartilage (Fig. 5G and fig. S5D). Ihh signaling is a crucial early regulator of chondrocyte hypertrophy and proliferation (*21*–*23*). To assess whether increased Ihh expression, a marker of prehypertrophy, was associated with progression to terminal hypertrophic differentiation, Runx2, collagen type X, and MMP13 protein expression were examined. Runx2 (Fig. 5, J and K, and fig. S5F) and MMP13 (fig. S7, A and B) expression were significantly increased in the Adseverin$^{-/-}$ versus Adseverin$^{+/+}$ mice. Collagen type X (Fig. 5L and fig. S5G) appeared increased in the articular cartilage of Adseverin$^{-/-}$ mice.

At 18 weeks, immunohistochemical staining revealed that adseverin-expressing chondrocytes began repopulating the articular cartilage despite initial tamoxifen treatment in Adseverin$^{-/-}$ mice (Fig. 6A and fig. S6A). However, although the number of adseverin-positive cells was more numerous than at 14 weeks, they remained significantly decreased in Adseverin$^{-/-}$ versus Adseverin$^{+/+}$ mice (Fig. 6B). Changes in Ihh expression were attenuated in association with the reappearance of adseverin expression as Ihh was significantly increased in the articular cartilage of only the MTP cartilage in Adseverin$^{-/-}$ mice (Fig. 6, C and D, and fig. S6B). In contrast, Ki67, on average, was lower but continued to be significantly increased in the cartilage of all knee compartments in the Adseverin$^{-/-}$ mice (Fig. 6, E and F, and fig. S6C). Aggrecan expression appeared diminished in the territorial and interterritorial matrix of the deep zone cartilage in the Adseverin$^{-/-}$ mice. This loss was especially apparent in the articular cartilage of the LFC and LTP (Fig. 6G and fig. S6D). There was still increased apoptosis in the articular cartilage and F-actin also appears to be reduced in chondrocytes of Adseverin$^{-/-}$ mice (Fig. 6, H and I, and fig. S6E). Consistent with the attenuation of Ihh expression, Runx2 (Fig. 6, J and K, and fig. S6F) was not significantly different between Adseverin$^{-/-}$ and Adseverin$^{+/+}$ mice. However, terminal hypertrophic molecule MMP13 (fig. S7, C and D) remains significantly increased and also collagen type X (Fig. 6L and fig. S6G) appeared increased in the articular cartilage of Adseverin$^{-/-}$ mice.

Adseverin$^{-/-}$ articular chondrocytes exhibit features of dedifferentiation and are unable to form viable articular cartilage tissues in vitro

Previous work has shown that adseverin knockdown in primary articular chondrocytes promotes dedifferentiation through actin polymerization in vitro (*13*). However, features of dedifferentiation were not present in Adseverin$^{-/-}$ chondrocytes of the native articular cartilage. This raised the question as to whether the changes were prevented by the surrounding ECM. For this reason, articular chondrocytes isolated from 10-week-old Adseverin$^{-/-}$ and Adseverin$^{+/+}$ mice were cultured in the monolayer to assess their phenotype. At day 3, phase contrast images revealed that Adseverin$^{-/-}$ chondrocytes acquired an elongated and spindle-shaped morphology compared to Adseverin$^{+/+}$ chondrocytes (Fig. 7A). Adseverin$^{-/-}$ chondrocytes developed actin stress fibers which increased by day 7 of monolayer culture (Fig. 7B) and was confirmed by the presence of decreased G-/F-actin ratio in these cells (Fig. 7C). There was no difference in the total amount of actin present in Adseverin$^{-/-}$ cells compared to controls (Fig. 7D). Expectedly, Adseverin$^{-/-}$ chondrocytes also appeared more proliferative compared to Adseverin$^{+/+}$ chondrocytes. Western blot analysis confirmed that adseverin protein expression remained depleted in Adseverin$^{-/-}$ cells (Fig. 7E).

Given earlier findings identified that markers of hypertrophy Ihh, Runx2, collagen type X, and MMP13 were significantly up-regulated in Adseverin$^{-/-}$ articular chondrocytes, it was postulated that these cells have a greater ability to mineralize. When the cells were grown under the mineralization-inducing condition of inorganic phosphate, by day 3 of this treatment, phase contrast microscopy revealed mineral accumulation in the Adseverin$^{-/-}$ chondrocyte cultures compared to the control (Fig. 7F). Von Kossa staining confirmed the increased deposition of calcium in Adseverin$^{-/-}$ versus Adseverin$^{+/+}$ chondrocytes (Fig. 7G).

To assess whether adseverin deletion affected the ability of articular chondrocytes to accumulate matrix, cells were seeded in three-dimensional (3D) membrane cultures to allow for cartilage tissue

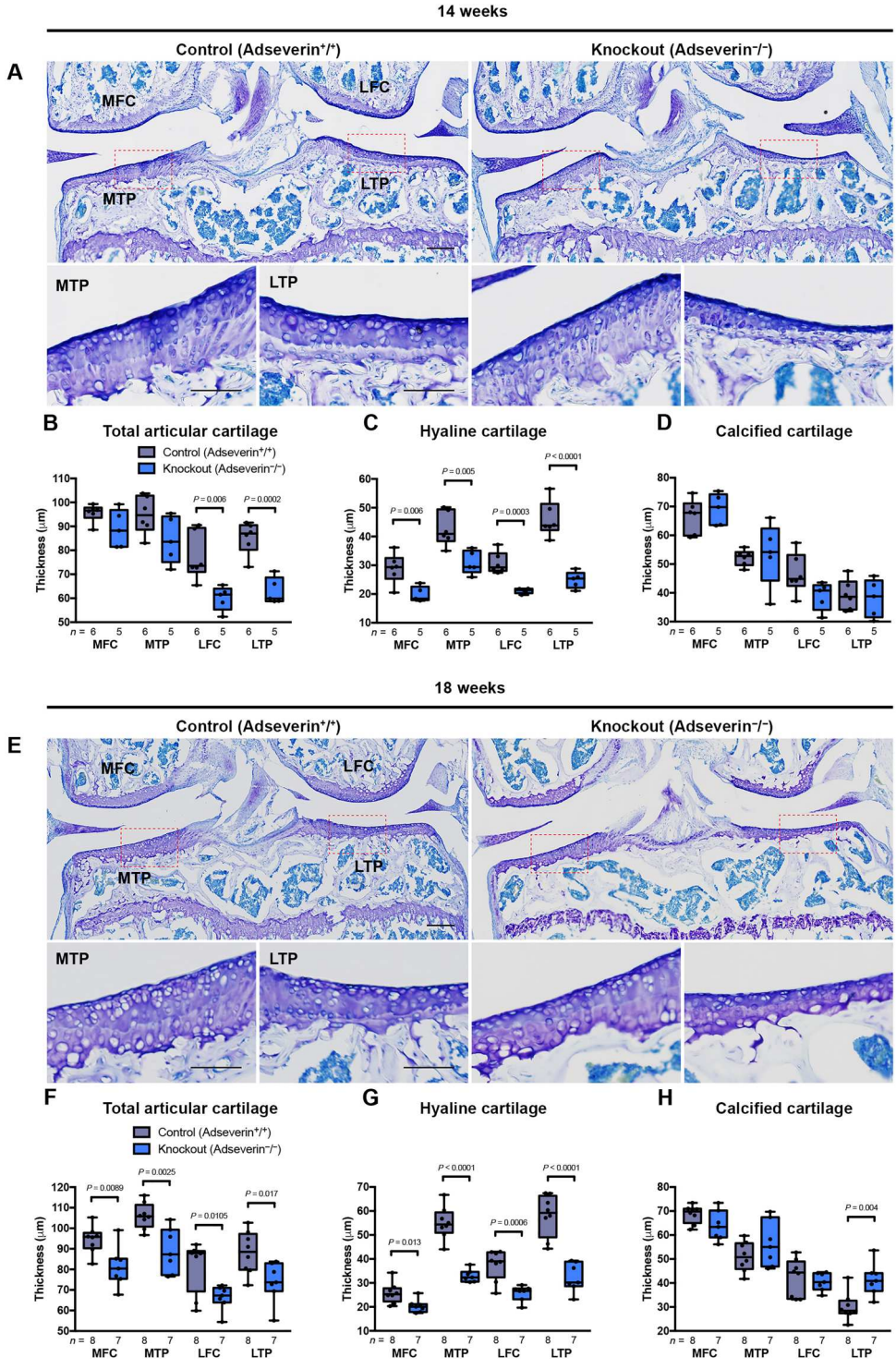

Fig. 4. Adseverin deletion results in progressive thinning of the hyaline component of articular cartilage. Toluidine blue–stained coronal sections of the knee joint of (**A**) 14- and (**E**) 18-week Adseverin$^{-/-}$ and Adseverin$^{+/+}$ mice. The bottom photomicrograph shows higher-magnification images of the indicated regions. Scale bars, 200 μm (lower magnification) and 100 μm (higher magnification). (**B** and **F**) Mean total articular, (**C** and **G**) hyaline, and (**D** and **H**) calcified cartilage thickness measurements of 14- and 18-week Adseverin$^{-/-}$ and Adseverin$^{+/+}$ mice. Box plots represent median values and interquartile ranges, and whiskers are plotted using the Tukey method. Statistical analysis was assessed using Student's unpaired two-tailed *t* test (B to D and F to H). The number of biological replicates in each group and *P* values are indicated in the figure.

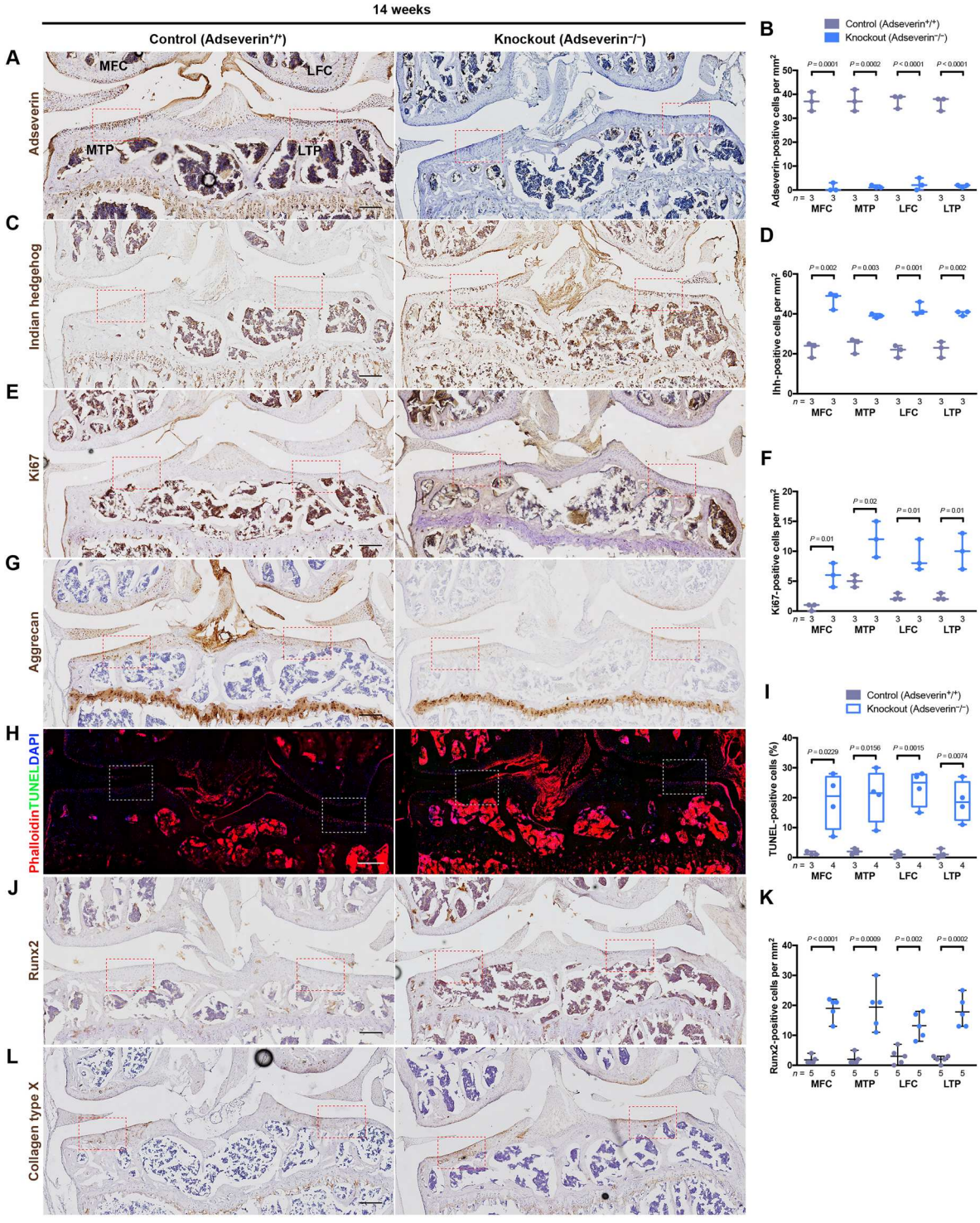

Fig. 5. Increased expression of Indian hedgehog, Ki67, apoptosis, hypertrophic markers, and decreased F-actin and aggrecan is maintained in Adseverin$^{-/-}$ articular cartilage. Immunohistochemical staining and quantification at 14 weeks of (**A** and **B**) adseverin, (**C** and **D**) Ihh, and (**E** and **F**) Ki67, as well as immunostaining for (**G**) aggrecan in the articular cartilage of Adseverin$^{-/-}$ versus Adseverin$^{+/+}$ mice. Scale bars, 200 μm. (**H**) Apoptotic chondrocytes and the actin cytoskeleton were detected by immunofluorescent staining with TUNEL (green) and phalloidin (red), respectively. DAPI (blue) stains nuclei. Scale bar, 400 μm. Higher-magnification images of the red or white dashed box in regions are in fig. S5. (**I**) Quantification of TUNEL-positive cells in the articular cartilage of Adseverin$^{-/-}$ and Adseverin$^{+/+}$ mice. Immunohistochemical staining for hypertrophic markers (**J**) Runx2 with (**K**) quantification and (**L**) collagen type X in the articular cartilage of Adseverin$^{-/-}$ versus Adseverin$^{+/+}$ mice. Dot plots represent the mean with minimum and maximum values. Box plots represent median values and interquartile ranges, and whiskers are plotted using the Tukey method. Statistical analysis was assessed using Student's unpaired two-tailed *t* test (B, D, F, I, and K). The number of biological replicates in each group and *P* values are indicated in the figure.

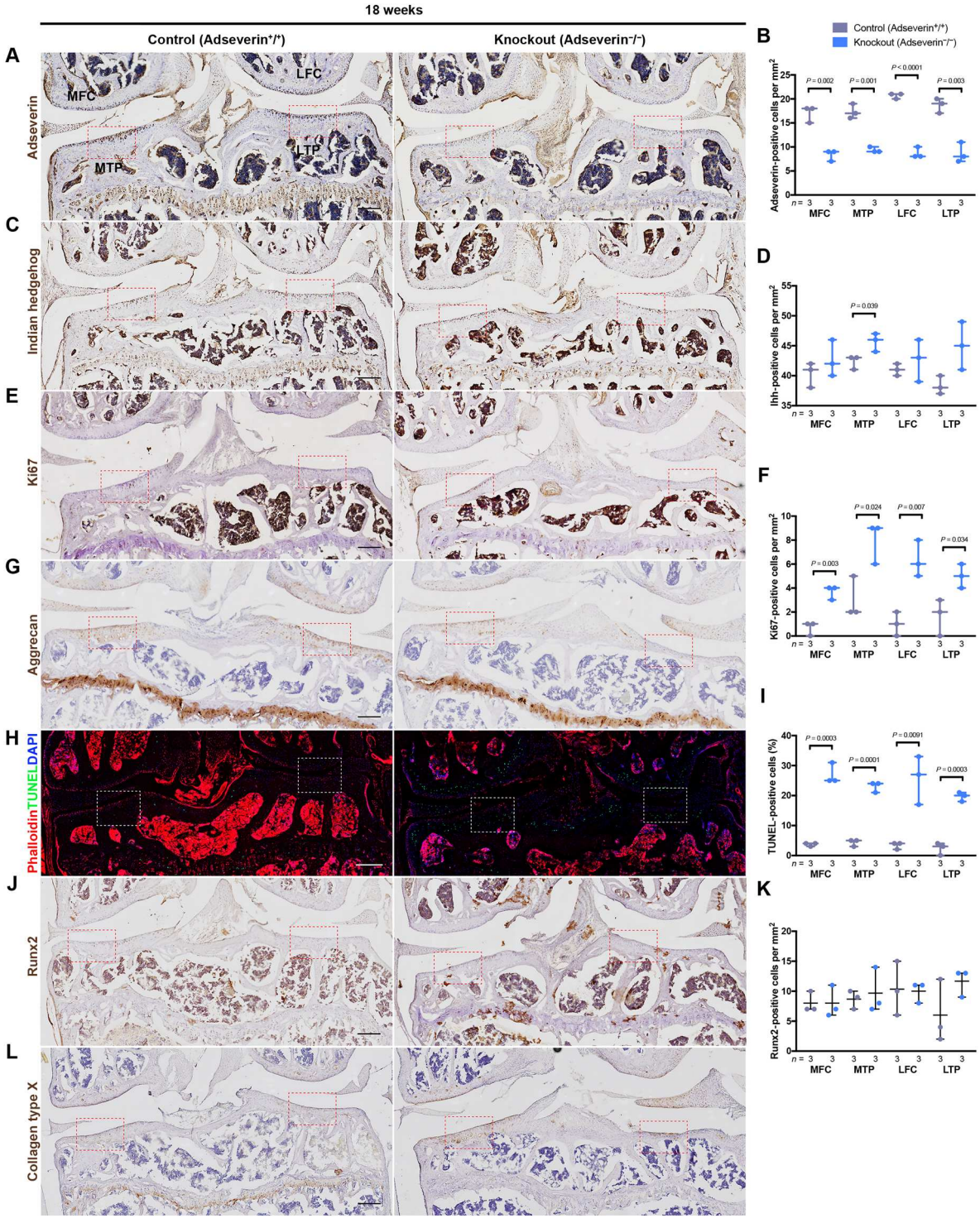

Fig. 6. Repopulation of adseverin-positive chondrocytes attenuated changes in Indian hedgehog and Runx2 expression despite increased proliferation, apoptosis, collagen type X, and decreased aggrecan and F-actin. Immunohistochemical staining and quantification at 18 weeks of (**A** and **B**) adseverin, (**C** and **D**) Ihh, and (**E** and **F**) Ki67, as well as immunostaining for (**G**) aggrecan in the articular cartilage of Adseverin$^{-/-}$ and Adseverin$^{+/+}$ mice. Scale bars, 200 μm. (**H**) Apoptotic chondrocytes and the actin cytoskeleton were detected by immunofluorescent staining with TUNEL (green) and phalloidin (red), respectively. DAPI (blue) stains nuclei. Scale bar, 400 μm. Higher-magnification images of the red or white dashed box in regions are in fig. S6. (**I**) Quantification of TUNEL-positive cells in the articular cartilage of Adseverin$^{-/-}$ and Adseverin$^{+/+}$ mice. Immunohistochemical staining of hypertrophic markers (**J**) Runx2 with (**K**) quantification and (**L**) collagen type X in the articular cartilage of Adseverin$^{-/-}$ versus Adseverin$^{+/+}$ mice. Dot plots represent the mean with minimum and maximum values. Statistical analysis was assessed using Student's unpaired two-tailed *t* test (B, D, F, I, and K). The number of biological replicates in each group and *P* values are indicated in the figure.

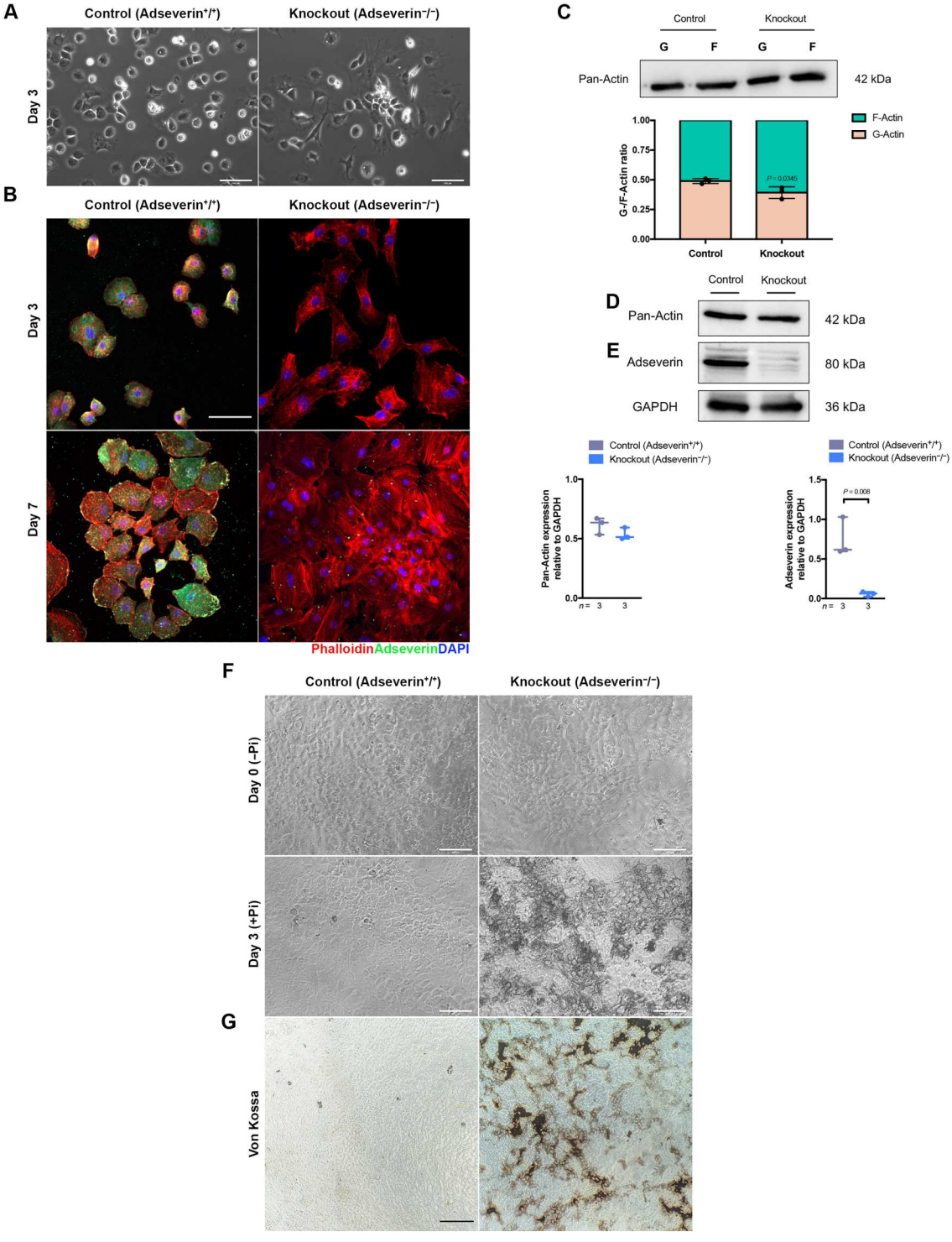

Fig. 7. Adseverin$^{-/-}$ articular chondrocytes exhibit features of dedifferentiation and enhanced mineralization potential in vitro. (**A**) Phase contrast images of primary articular chondrocytes in monolayer culture for 3 days after isolation from Adseverin$^{-/-}$ and Adseverin$^{+/+}$ 10-week-old mice. Scale bars, 100 μm (**B**) Immunofluorescent images of phalloidin (red), adseverin (green), and DAPI (blue) in primary articular chondrocytes in monolayer culture for 3 and 7 days after isolation from Adseverin$^{-/-}$ and Adseverin$^{+/+}$ mice at 10 weeks of age. Scale bar, 50 μm. (**C**) Western blot densitometry analysis of G-/F-actin ratio, (**D**) pan-actin, and (**E**) adseverin of primary articular chondrocytes in monolayer culture for 3 days after isolation from Adseverin$^{-/-}$ and Adseverin$^{+/+}$ mice at 10 weeks of age. Error bars represent mean ± SEM of n = 3 independent experiments. Phase contrast image of (**F**) cells at day 0 (at the time of starting phosphate supplementation) and (**G** and **H**) phase contrast and Von Kossa stained images following 3 days of phosphate treatment of primary articular chondrocytes from Adseverin$^{-/-}$ and Adseverin$^{+/+}$ mice at 10 weeks of age in monolayer culture treated with inorganic phosphate (1 mM) for 3 days. Scale bars, 100 μm. Statistical analysis was assessed using Student's unpaired two-tailed t test (C to E). The number of biological replicates in each group and P values are indicated in the figure.

formation. Compared to Adseverin$^{+/+}$ tissues, histological assessment revealed that Adseverin$^{-/-}$ tissues exhibit loss of cell viability and tissue. There was minimal focal proteoglycan accumulation (Fig. 8, A and B). Immunohistochemistry shows the presence of small amounts of aggrecan (Fig. 8C) and collagen type II (Fig. 8D) in the cartilage tissues formed by Adseverin$^{-/-}$ chondrocytes. In contrast, there was greater accumulation of collagen type I which was distributed uniformly across the entire tissue formed by Adseverin$^{-/-}$ versus Adseverin$^{+/+}$ chondrocytes (Fig. 8E). Biochemical analysis shows that Adseverin$^{-/-}$ chondrocyte–formed tissues had significantly decreased sulfated glycosaminoglycan and DNA contents relative to Adseverin$^{+/+}$ tissues (Fig. 8F). Gene set enrichment analysis of RNA-seq data revealed that Adseverin$^{-/-}$ articular chondrocytes at 10 weeks showed significantly down-regulated ECM interactions and mitochondrial function and significantly up-regulated DNA repair gene sets (Fig. 8G) which may contribute to these changes.

Adseverin deletion enhances OA severity

Considering all the changes induced by adseverin deletion, it was postulated that they should influence OA severity. To investigate this, 10-week-old Adseverin$^{-/-}$ and Adseverin$^{+/+}$ underwent DMM (Fig. 9A). At 4 weeks after DMM (14 weeks), histological analysis revealed OA changes in the medial compartment of both Adseverin$^{-/-}$ and Adseverin$^{+/+}$ mice (Fig. 9B and fig. S8A). Average osteophyte size and maturity scores were not significantly different between Adseverin$^{-/-}$ versus Adseverin$^{+/+}$ mice (fig. S8G). In keeping with this, there were no significant differences in OARSI scores between Adseverin$^{-/-}$ and Adseverin$^{+/+}$ mice (Fig. 9C). TUNEL analysis shows that Adseverin$^{-/-}$ mice had a significantly increased number of apoptotic cells in the articular cartilage of the MFC, MTP, and LFC. Phalloidin staining revealed F-actin loss in the articular chondrocytes of all compartments of the knee joint compared to Adseverin$^{+/+}$ mice (Fig. 9, D and E, and fig. S8B). As expected, adseverin expression in Adseverin$^{-/-}$ articular cartilage remains significantly decreased (Fig. 9, F and G, and fig. S8C).

At 8 weeks after DMM (18 weeks), histological examination revealed more severe OA change with tissue erosion to the calcified cartilage that often involved more than 75% of the articular surface of the MTP and MFC of the Adseverin$^{-/-}$ mice. OA changes characterized by fibrillation and loss of proteoglycans and osteophyte formation were also present in the LTP cartilage of these mice (Fig. 9H and fig. S8D). Osteophyte size scores were significantly increased only for the MTP and LTP and osteophyte maturity scores were significantly increased for the LFC and LTP in Adseverin$^{-/-}$ compared to Adseverin$^{+/+}$ mice (fig. S8H). OARSI scores of Adseverin$^{-/-}$ were significantly higher in the MTP and LTP versus Adseverin$^{+/+}$ mice (Fig. 9I). TUNEL analysis shows that Adseverin$^{-/-}$ had a significantly increased number of apoptotic cells in the cartilage of the MFC, LFC, and LTP. F-actin loss was comparable in the medial compartment and markedly reduced in the LTP between Adseverin$^{-/-}$ and Adseverin$^{+/+}$ mice (Fig. 9, J and K, and fig. S8E). Adseverin expression was low but not significantly different in the MFC and MTP and was significantly decreased in the LFC and LTP to levels present in the medial compartment in Adseverin$^{-/-}$ versus Adseverin$^{+/+}$ mice (Fig. 9, L and M, and fig. S8F).

Adseverin deletion promotes postnatal growth plate thinning and decreased hypertrophic differentiation

As adseverin expression was also depleted in postnatal growth plate chondrocytes (Fig. 2D), histomorphometry and immunohistochemical assessments were performed in the tibial growth plate. Postnatal growth plate length was measured at 10, 14, and 18 weeks (fig. S9, A to D) and revealed significant decreases in growth plate length over time (fig. S9, E to G) in Adseverin$^{-/-}$ versus Adseverin$^{+/+}$ mice. These changes were associated with decreased cellularity (fig. S9H) and Ki67 expression (fig. S9I) and increased apoptosis (fig. S9J).

In the tibial growth plate, loss of adseverin in chondrocytes resulted in a significant decrease in Runx2 expression at 14 and 18 weeks (fig. S10, A and B) in Adseverin$^{-/-}$ versus Adseverin$^{+/+}$ mice. Furthermore, collagen type X was substantially decreased in the hypertrophic zone at 18 weeks (fig. S10C) and MMP13 was significantly decreased at 14 weeks (fig. S10, D and E) in Adseverin$^{-/-}$ mice.

DISCUSSION

This study expands our investigations of the role of adseverin in vivo and in vitro in the regulation of articular chondrocyte phenotype and its contributions to tissue homeostasis and OA progression. IL-1β and TNF-α are important mediators in OA pathogenesis and can promote the phenotypic shift that occurs in this disease process (*14*, *15*, *24*, *25*). The data demonstrated that IL-1β and not TNF-α leads to significant down-regulation of adseverin levels in bovine primary articular chondrocytes in vitro. As these were in vitro studies and IL-1β exposure is not responsible for all the OA changes that develop, the relationship between OA and adseverin expression in vivo was examined using the DMM mouse OA model. These mice, as expected, developed OA changes in the cartilage of the medial compartment (MFC and MTP). The chondrocytes had decreased adseverin expression not only in the affected area but also in the lateral compartment cartilage which did not show macroscopic or histological evidence of degradation. This suggests that adseverin loss precedes the development of OA cartilage changes and perhaps as our data suggest, this may be due to factors such as pro-inflammatory cytokines e.g., IL-1β, which are known to be present in the mouse OA model (*26*). OA severity in the DMM model has been reported by others to be sex-dependent (*27*) and, in this study, female mice exhibited delayed adseverin loss that correlated with OA severity (figs. S11 and S12). Given all of these findings, we next explored the contributions of adseverin to chondrocyte phenotype and cartilage tissue homeostasis by evaluating the cartilage changes early after adseverin deletion. At 10 weeks, there were cell and matrix changes, including chondrocyte death and reduction of F-actin in the absence of OA cartilage changes. This occurred in both female (fig. S13) and male mice. RNA-seq analysis showed that adseverin deletion induced changes indicative of chondrocyte prehypertrophy and cellular stress response as signaling pathways associated with Ihh, proliferation, and DNA repair were up-regulated, and actin cytoskeleton organization, mitochondrial function, and ECM interactions were down-regulated. Selected genes identified by RNA-seq as differentially expressed were confirmed by immunohistochemistry studies which showed that Ihh and Ki67 were significantly increased and aggrecan was decreased following adseverin deletion. These

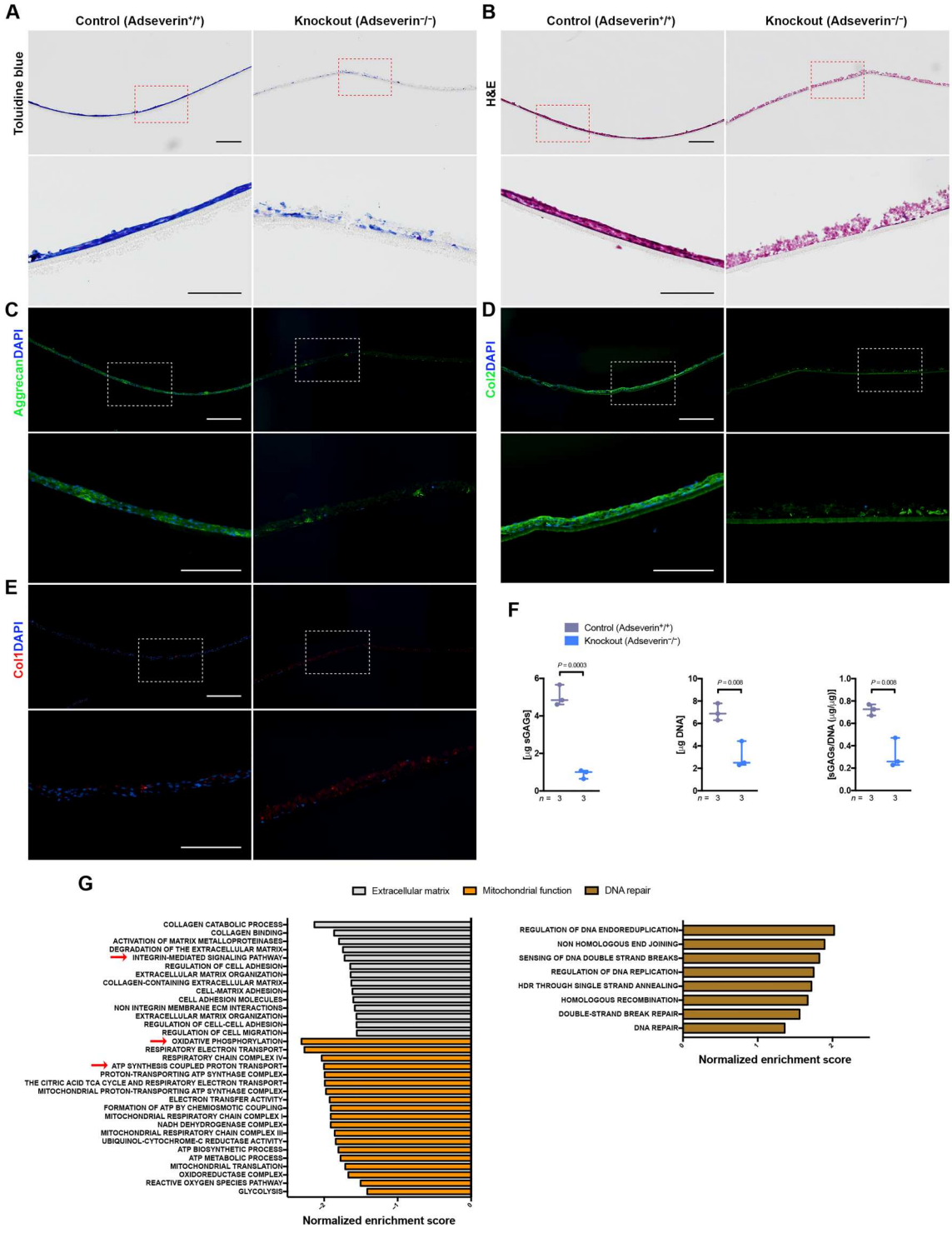

Fig. 8. Adseverin$^{-/-}$ articular chondrocytes are unable to grow tissues that remain viable in vitro. Histological appearance of (**A**) toluidine blue– and (**B**) H&E-stained in vitro cartilage tissues formed by Adseverin$^{-/-}$ and Adseverin$^{+/+}$ primary articular chondrocytes after 2 weeks of 3D membrane culture. The bottom photomicrograph shows higher-magnification images of the indicated regions. Scale bar, 200 µm (lower magnification) and 100 µm (higher magnification). Immunohistochemical staining for (**C**) aggrecan, (**D**) collagen type I (Col1), and (**E**) collagen type II (Col2) in the in vitro formed cartilage tissues. The bottom photomicrograph shows higher-magnification images of the indicated regions. Scale bars, 200 µm (lower magnification) and 100 µm (higher magnification). (**F**) Biochemical analysis of sulfated glycosaminoglycans and DNA of the in vitro formed cartilage tissues. (**G**) Gene set enrichment analysis and functional grouping of gene sets associated with extracellular matrix interactions, mitochondrial function, and DNA repair from RNA-seq data of Adseverin$^{-/-}$ versus Adseverin$^{+/+}$ articular chondrocytes isolated from 10-week-old mice. Statistical analysis was assessed using Student's unpaired two-tailed *t* test (F). The number of biological replicates in each group and *P* values are indicated in the figure. Experiments were repeated three times (A to E) from independent cell isolations with similar results.

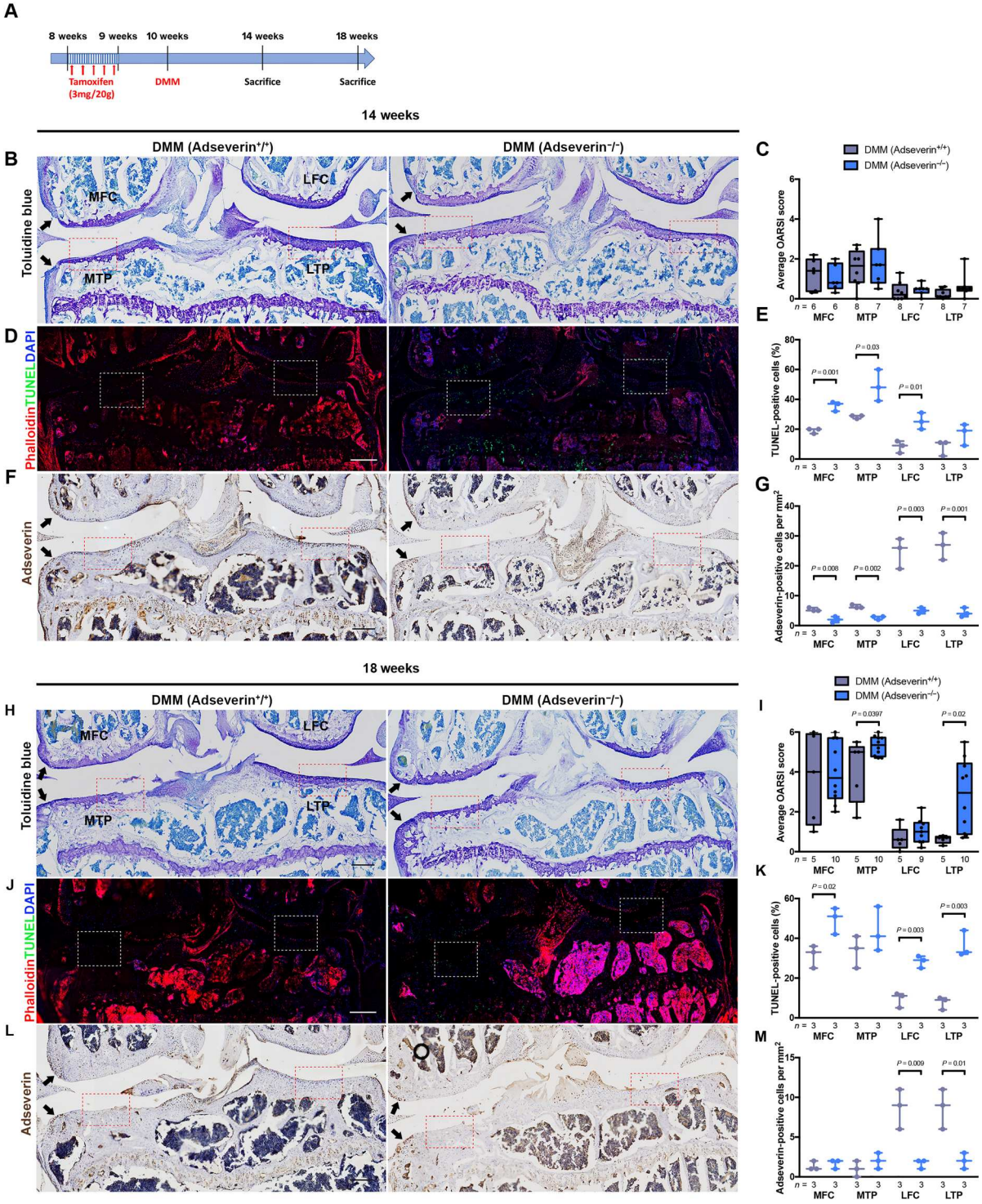

Fig. 9. Adseverin$^{-/-}$ mice develop greater OA severity. (**A**) Schematic tamoxifen-induced adseverin deletion and DMM timeline. OA severity induced by DMM surgery of Adseverin$^{-/-}$ and Adseverin$^{+/+}$ mice at 14 (**B**) and 18 weeks (**H**) was assessed by histological assessment of toluidine blue–stained coronal sections of the mouse knee joint. The black arrow indicates osteophyte. Scale bars, 200 μm. (**C** and **I**) Mean OARSI scores. (**F** and **L**) Immunohistochemical staining and (**G** and **M**) quantification of adseverin-positive cells in the articular cartilage of Adseverin$^{-/-}$ and Adseverin$^{+/+}$ mice after DMM surgery. Scale bars, 200 μm. (**D** and **J**) Fluorescent images of apoptotic chondrocytes and the actin cytoskeleton following immunofluorescent staining with TUNEL (green) or phalloidin (red), respectively. DAPI (blue) stains nuclei. Scale bars, 400 μm. Higher-magnification images of the red or white dashed box regions are in fig. S8. (**E** and **K**) Quantification of TUNEL-positive cells in the articular cartilage of Adseverin$^{-/-}$ and Adseverin$^{+/+}$ mice after DMM surgery. Box plots represent median values and interquartile ranges, and whiskers are plotted using the Tukey method. Dot plots represent the mean with minimum and maximum values. Statistical analysis was assessed using Student's unpaired two-tailed *t* test (C, E, G, I, K, and M). The number of biological replicates in each group and *P* values are indicated in the figure.

alterations were associated with increased cartilage stiffness and later thinner hyaline and thicker calcified cartilage zones and increased hypertrophic differentiation indicated by Runx2, collagen type X, and MMP13. αSMA is correlated with increased ECM stiffness (*28*, *29*) and OA (*5*) and was significantly up-regulated with adseverin deletion (fig. S14). The increased Ihh and Runx2 expression induced by adseverin deletion appeared attenuated when adseverin re-expression occurred. However, terminal hypertrophic molecules collagen type X and MMP13 remained increased. Mouse Adseverin$^{-/-}$ chondrocytes grown in monolayer culture exhibited morphological and actin cytoskeletal changes and the ability to mineralize. These cells form cartilage-like tissue in vitro but the tissue did not remain viable, which demonstrates the functional consequence of deletion of adseverin. In light of these findings, the effect of DMM on Adseverin$^{-/-}$ mice was examined. These mice develop accelerated OA indicated by cartilage degradation and osteophyte formation in both the medial and lateral compartments of the knee joint compared to controls which showed degradation and osteophyte formation only in the medial compartment. These findings demonstrate the importance of adseverin in maintaining articular cartilage homeostasis by preventing chondrocyte differentiation toward the hypertrophic phenotype. Human early OA chondrocytes demonstrated a lack of adseverin in the upper aspect of cartilage, F-actin loss, and the expression of Ihh throughout the cartilage (fig. S15), which were some of the changes detected in the mouse cartilage with adseverin deletion.

The decrease in F-actin due to adseverin deletion in articular chondrocytes resembles the actin changes observed in OA chondrocytes and suggests that an OA phenotype, at least in part, is a consequence of actin cytoskeleton modifications (*8*). The change in F-actin organization in OA chondrocytes is not well defined but cells show reduced phalloidin staining (*30*, *31*), and findings from several studies attributed this reduction and/or disassembled appearance of F-actin to IL-1 exposure (*32*, *33*). In keeping with this, we observed that IL-1β treatment down-regulated adseverin expression in bovine chondrocytes. IL-1β is known to be elevated in the DMM model of OA (*26*), which could explain the decreased adseverin throughout the cartilage in the joints of DMM mice. We also observed that, shortly after adseverin deletion, F-actin is reduced in mid/deep zone chondrocytes, along with increased cell death. Reduction of F-actin and adseverin expression appears to precede morphological cartilage matrix changes. Others have also shown that biochemical changes occur in normal-appearing cartilage early in OA (*34*). This suggests that adseverin and F-actin reduction may serve as early markers of OA. Although the disassembly of F-actin in OA chondrocytes is mediated by adseverin loss, it is likely not dependent solely on adseverin as results from RNA-seq analysis indicate that other actin-binding proteins, such as WASP/WAVE or Arp2/3 complex, were down-regulated and may also be involved. Thus, actin-binding proteins like adseverin play a role in preserving F-actin organization (*35*) and are critical for maintaining chondrocyte phenotype and articular cartilage homeostasis.

As expected, the increased apoptosis seen in DMM models and human OA was also present in our DMM mouse model of OA (*4*). However, the increased apoptosis due to adseverin deletion was unexpected and may be the result of an altered actin cytoskeleton status. Studies have demonstrated that, using jasplakinolide, an F-actin–stabilizing drug that promotes actin polymerization (*36*) resulted in apoptosis in various cell types (*37*, *38*). Jasplakinolide can also increase deoxyribonuclease (DNase) I activity, which is involved in the degradation of nuclear DNA strands during apoptosis (*39*, *40*). DNase I binds with high affinity with G-actin monomers (*40*); thus, if the cells contain predominately F-actin, then this may deplete the G-actin pool to free DNase I. Given that adseverin knockdown (*13*) and deletion (current study) in vitro promote actin polymerization evidenced by decreased G-/F-actin ratio, it is possible that free DNase I may be contributing to the increased apoptosis observed in Adseverin$^{-/-}$ chondrocytes. Alternatively, F-actin stabilization can also promote apoptosis by prolonging the opening of voltage-dependent anion channels (VDAC) on the outer mitochondria membrane. This leads to the loss of mitochondrial membrane potential and the subsequent release of cytochrome c (*41*). Although the loss of mitochondrial membrane potential was not evaluated in the current study, the RNA-seq results suggest that there is mitochondrial dysfunction, which could result in mitochondrial membrane potential loss (*42*). Alterations in levels of actin-binding proteins can also increase apoptosis (*43*). For example, gelsolin, an actin-binding protein, has been demonstrated to have a prosurvival role by preventing apoptosis (*44*) by inhibiting VDAC pore opening (*45*). Given that adseverin is a member of the gelsolin superfamily and shares the highest degree of homology with gelsolin (*46*), adseverin could play a similar role in preventing apoptosis. This is evidenced by our RNA-seq data indicating that both VDAC1 and hexokinase 2 (HK2) were significantly down-regulated following adseverin deletion (fig. S3B). The association of VDAC1 and HK2 on the outer mitochondrial membrane has been well established to regulate the apoptotic responsiveness of the cell (*47*). Our findings suggest that adseverin contributes to apoptosis resistance in chondrocytes; however, it is still unclear if the down-regulation of VDAC1 and HK2 is a primary consequence of adseverin loss or secondary to actin cytoskeleton changes.

Adseverin deletion in articular chondrocytes increased Ihh expression. Ihh normally is expressed by prehypertrophic chondrocytes and is an essential regulator of chondrocyte hypertrophy, proliferation, and mechanotransduction (*21*, *23*, *48*). However, when Ihh is aberrantly activated in OA (*1*, *49*), it results in the abnormal hypertrophic differentiation of articular chondrocytes leading to cartilage degradation due to altered tissue homeostasis (*50*). Studies have shown that Ihh signaling pathway disruption can attenuate OA severity (*51*, *52*), thus implicating it in OA development in the DMM OA mouse model. Although Ihh regulates the progression of chondrocyte hypertrophy, our RNA-seq analysis indicates that adseverin deletion promotes an early prehypertrophic phenotype. This was evidenced by the profile of genes up-regulated such as Ihh, Ptch1, and Hhip. Markers of proliferation Ki67, Ccne1, and Cdc6 were also up-regulated which indicates Ihh signaling activation (*48*). These proliferative changes may be regulated through Gas1 as it has been shown to mediate hedgehog-dependent proliferation (*53*) and was significantly decreased with adseverin deletion. Studies have shown that Gas1 is a critical component in promoting hedgehog signaling and is down-regulated as hedgehog signaling levels increase (*54*, *55*). Transcriptional down-regulation of Gas1 and up-regulation of Hhip, positive and negative hedgehog signaling components, respectively allow the cell to tightly control, through multiple mechanisms, the amount of hedgehog signal necessary for promoting proliferation and hypertrophy observed in Adseverin$^{-/-}$ articular chondrocytes. Genes associated with terminal hypertrophic differentiation such as MMP13, Runx2, and collagen

type X were not significantly altered at the early 10-week time point. However, this prehypertrophy leads to progression to hypertrophic differentiation as Adseverin$^{-/-}$ articular chondrocytes acquire hypertrophic-like features such as increased Runx2, collagen type X, and MMP13 expression, increased mineralization potential in vitro, increased apoptosis in vivo, and can be associated with increased calcified cartilage thickness in mice at a later time point.

Together, our findings indicate that adseverin prevents articular chondrocyte hypertrophy through modulation of Ihh expression. This differs from the study by Nurminsky *et al*. (*56*) who, using fetal growth plate chondrocytes, demonstrate that adseverin overexpression promotes chondrocyte hypertrophy and up-regulation of Ihh; however, this may be due to differences in adseverin function in growth plate versus articular chondrocytes studied in the current study. Our data show that adseverin deletion induces several changes in the postnatal growth plate that differs from changes observed in the articular cartilage. We observed evidence of growth plate thinning over time following adseverin deletion (fig. S9, A to C and E to G). This was associated with significantly decreased cellularity (fig. S9H) and Ki67 expression (fig. S9I) and increased apoptosis (fig. S9J). Most notably, adseverin deletion decreases growth plate chondrocyte hypertrophy as Runx2 (fig. S10, A and B), collagen type X (fig. S10C), and MMP13 (fig. S10, D and E) were significantly decreased. These findings reveal that adseverin deletion promotes hypertrophic differentiation in the articular chondrocytes, whereas hypertrophy is prevented in the postnatal growth plate chondrocytes and is in keeping with the observations reported by Nurminsky *et al*. (*56*).

Although it remains unclear how adseverin deletion led to increased Ihh expression, it may be due to mechanical overloading, also a proposed mechanism of OA development (*50*). Given that the actin cytoskeleton mediates mechanotransduction (*57*), it is possible that the actin changes induced by adseverin deletion may have compromised the mechanosensitivity of articular chondrocytes resulting in perceiving physiological mechanical load as overload leading to increased Ihh signaling. Primary cilium present on chondrocytes has been shown to transduce mechanical loading and regulate Ihh signaling via actin (*58*). Alternatively, it may be that the decreased amount of aggrecan, the major cartilage proteoglycan, resulted in altered biomechanical properties of the cartilage and influenced how mechanical load is transmitted throughout the tissue. This could be another contributing factor, independent of actin changes induced by adseverin loss, in affecting chondrocyte response to mechanical loading and leading to increased Ihh expression and apoptosis (*59*). Further study is required to identify which or if both mechanisms are responsible.

The decreased expression of aggrecan may be due to the up-regulation of Ihh which has been shown by others to decrease articular cartilage thickness and proteoglycan content through Wnt/β-catenin and bone morphogenetic protein signaling (*60*). The correlation between increased cartilage stiffness and decreased aggrecan expression has been shown to be associated with aging and OA development by others (*18*, *20*). Furthermore, thinning of the articular cartilage has been reported by others (*61*) to be associated with decreased aggrecan and has been demonstrated to predispose the joint to OA development and exacerbate OA severity (*62*). Together, these findings suggest that the changes induced by adseverin deletion predispose the articular cartilage to OA damage and may explain why adseverin-deleted mice had increased OA severity with DMM. Disturbances in the ECM composition due to adseverin deletion can also compromise cell-matrix interactions, which can be mediated by the actin cytoskeleton, and is important for chondrocyte function. This includes matrix remodeling, mechanotransduction, and cell survival (*63*). Our RNA-seq data indicate that key cell-matrix interactions such as integrin-mediated signaling are significantly impaired with adseverin deletion. This was also associated with the down-regulation of mitochondrial function and the up-regulation of DNA repair gene sets. Loss of these cell-matrix interactions could initiate anoikis, a form of programmed cell death that occurs when cell-matrix interactions are lost (*64*), and may be inducing a cellular stress response that is consequently responsible for the abnormal matrix accumulation and compromised cell viability observed in Adseverin$^{-/-}$ in vitro articular cartilage tissues. This may also contribute to F-actin reduction and increased apoptosis observed in the mouse native articular cartilage with adseverin deletion.

A finding that was not anticipated in the current study was the re-expression of adseverin in chondrocytes at 18 weeks. It is unclear why this occurred but we postulate that these cells may be derived from an endogenous population of articular cartilage progenitor cells or chondroprogenitors (*65*). These cells are normally quiescent and are described to be similar to mesenchymal stromal cells (MSCs). Chondroprogenitors have the ability to migrate toward the site of cartilage damage and differentiate into articular chondrocytes to maintain tissue homeostasis. It is possible that these cells do not express aggrecan at the time of tamoxifen administration, thus escaping adseverin deletion. This hypothesis is supported by the presence of osteophytes, which are derived from chondroprogenitors or MSCs in the periosteum (*66*), which had cells that stained for adseverin in the Adseverin$^{-/-}$ mice (Fig. 9, F and L). The mechanism leading to the activation of these cells is not fully delineated, but the RNA-seq results would suggest that this might involve chondrocyte stress and death (*67*) as indicated by the up-regulation of DNA repair and the down-regulation of mitochondrial function pathways. This requires further investigation.

There are several potential limitations of this study. First, findings from other studies (*18*, *62*) suggest that the changes resulting from adseverin deletion should lead to the development of spontaneous age-related OA in the mice. This could not be determined due to the re-expression of adseverin in chondrocytes that occurs over time in Adseverin$^{-/-}$ mice. Second, although we report that F-actin is reduced as a result of adseverin deletion, it is possible that there are actin changes not captured at our current imaging resolution but may be detectable using super-resolution imaging techniques (*68*). Third, we note that adseverin deletion may result in changes that are occurring at the biochemical level that are not identified by transcriptome analysis. Fourth, another limitation was the 10-week time point chosen for the transcriptomic profiling, which precluded the evaluation of the acute effects of adseverin deletion. Fifth, although we have highlighted sex-specific differences in the DMM mouse model in this study, these differences were not assessed in humans. Last, additional quantitative analysis such as Western blot for proteins assessed by immunohistochemical studies could not be done due to the limited number of cells that can be isolated from the small amount of adult mouse articular cartilage.

In summary, this study confirms the critical role of adseverin in regulating chondrocyte phenotype and cartilage homeostasis by

preventing chondrocyte hypertrophy and thus OA progression. RNA-seq did not show an increase in expression levels of other actin-binding proteins to compensate for adseverin loss. Our data demonstrate that adseverin loss also compromises the viability (increased apoptosis) and function (reduction in aggrecan proteoglycan and the inability to form viable cartilage tissue in vitro) of articular chondrocytes. This alters ECM composition and compromises the biomechanical properties of cartilage (increased Young's modulus) which likely then influences the response of chondrocytes to mechanical loading (increased Ihh and subsequently hypertrophic differentiation) and contributing to OA progression by predisposing articular cartilage to enhanced degradation. Future work will focus on identifying the mechanisms that regulate adseverin expression in articular chondrocytes.

MATERIALS AND METHODS

Primary culture of articular chondrocytes

For bovine chondrocyte cultures, full-thickness articular chondrocytes were isolated from cartilage obtained from the metacarpophalangeal joint as previously described (*13*). Primary chondrocytes were seeded at 5×10^4 cells/cm^2 in serum-free Ham's F12 media for 24 hours. Cells were washed with phosphate-buffered saline (PBS) and fresh complete media [Ham's F12 with 5% fetal bovine serum (FBS) and 1% antimycotic/biotic] was added containing IL-1β (either 2.5 or 5 ng/ml; RP0106B-005, Kingfisher Biotech) or TNF-α (5 or 10 ng/ml; 2279-BT, R&D Systems). As the control, cells were cultured in complete media containing the vehicle, PBS.

Relative real-time qPCR

Primary bovine articular chondrocytes were harvested 24 hours after IL-1β or TNF-α treatment. Total RNA was extracted using TRIzol according to the manufacturer's directions and qPCR was performed as previously described (*13*). The primer names and sequences are listed in table S1.

Destabilization of medial meniscus surgical induction of osteoarthritis

All animal experiments were approved and carried out in accordance with the guidelines and policies of the University of Toronto Animal Care Committee (protocol #20012268). Surgery with a standard sterile technique was performed on the right knee of mice to induce OA in 10-week-old mice (*26*). Mice were randomly assigned into either sham or DMM groups with termination time points 4 and 8 weeks after surgery. For analgesia, meloxicam (2 mg/kg) and buprenorphine-sustained release (1 mg/kg) were injected subcutaneously before the operation, followed by another dose of meloxicam 24 hours after the operation. Mice were anesthetized and maintained with 3% inhalant isoflurane delivered with 100% O_2 (1 liter/min) via face mask. The entire right hind limb was shaved and cleaned by applying betadine solution followed by isopropyl alcohol twice. Mice were then placed on a warm circulating water pad to maintain the body temperature during the operation. A sterile drape was fitted over the entire animal and only the right knee was exposed. The surgery began with a 1 cm longitudinal skin incision originating from the distal femur and extending to the proximal tibia on the medial side of the knee. After locating the patellar tendon, a medial parapatellar longitudinal incision was made in the joint capsule. Dumont #4 forceps were used to laterally dislocate the patella and patellar ligament to expose the joint space. The fat pad was temporarily displaced laterally to expose the medial meniscotibial ligament which was then grasped by Dumont #4 forceps and rotated medially to rupture the ligament (akin to a traumatic injury). The medial meniscus was subsequently confirmed to be freely moving and macroscopically undamaged before relocating the fat pad and patella. The joint capsule was closed with a continuous suture using 6-0 absorbable Vicryl (Ethicon, Canada), and the subcutaneous layer and skin were closed with interrupted sutures. The tissue adhesive Vetbond (3M, USA) was applied to reinforce wound closure. Sham operations involved the same incision approach and visualization of the medial meniscotibial ligament without rupture of the ligament. After surgery, mice were returned to their home cage and allowed unrestricted movement and access to food and water.

Generation of adseverin conditional knockout mice

Adseverin$^{LoxP/LoxP}$ mice were provided by M. Glogauer (University of Toronto, Canada) (*69*). Agc1$^{tm(IRES\text{-}CreERT2)}$ (JAX, stock #019148) (*70*) and Adseverin$^{LoxP/LoxP}$ mice were mated to generate Agc1$^{tm(IRES\text{-}CreERT2)}$;Adseverin$^{WT/LoxP}$ mice. These resulting mice were then back-crossed with Adseverin$^{LoxP/LoxP}$ to generate littermates Agc1$^{tm(IRES\text{-}CreERT2)}$;Adseverin$^{LoxP/LoxP}$ and Adseverin$^{LoxP/LoxP}$, which are denoted respectively as knockout (Adseverin$^{-/-}$) and control (Adseverin$^{+/+}$) in this study. Both Agc1$^{tm(IRES\text{-}CreERT2)}$ and Adseverin$^{LoxP/LoxP}$ strains are in the C57BL/6J background. Both female and male mice were used in this study. The data from male mice are presented in the text and the data from the female mice are presented in the supplementary figures.

Tamoxifen induction of recombination

Tamoxifen (20 mg/ml; Sigma-Aldrich, Canada) was first dissolved in sterile 100% ethanol, and then diluted with sterile corn oil (Sigma-Aldrich, Canada) to result in a 9:1 corn oil–ethanol solution. One and a half milligrams of tamoxifen per 10 g of body weight was administered to 8-week-old mice by oral gavage once daily for five consecutive days. Mice at 10 weeks old were either euthanized for adseverin knockout analysis or underwent surgery.

Genotyping transgenic mice with polymerase chain reaction

The genotype of transgenic mice was determined by PCR analysis of DNA isolated from mouse tail tissue. DNA was extracted using 100 μl of DirectPCR lysis reagent (102-T, Viagen Biotech) supplemented with proteinase K (0.2 mg/ml; Sigma-Aldrich) per tail sample and incubated at 56°C water bath overnight. Samples were then incubated in an 86°C water bath for 1 hour to inactivate proteinase K. PCR was performed to confirm the genotype by assessing the presence of Cre and loxP transgene in the genomic DNA. The primer pair used for genotyping are as follows: Cre-F (5′-GAGTG ATGAGGTTCGCAAGA-3′) and Cre-R (5′-CTACACCAGAGAC GGAAATC-3′) for the presence of Cre [635 base pairs (bp)]. SCAD3 (5′-GTTAGTATTCCTCACTGGCACCC-3′) and Ads-SDL2 (5′-ATGTTTCAGGACAGGAGTCTGAGC-3′) for the presence of loxP allele. One band represents the wild-type allele (289 bp) and the other represents the loxP allele (363 bp). The presence of both bands indicates that the mouse is heterozygous for the loxP allele. To confirm whether successful Cre recombination and the deletion of adseverin exon 2 occurred, the following primers were

used: SCAD3 (5′-GTTAGTATTCCTCACTGGCACCC-3′) and Ads-NDEL2 (5′-GAACCCATGATCCTATTGCCTCAACC-3′) to detect the deletion band (509 bp). PCR reactions were performed using Platinum II Hot-Start Green PCR Master Mix (2X) (Thermo Fisher Scientific) according to the manufacturer′s protocol.

Histology and immunohistochemistry

Animals were euthanized by CO_2 at 10 (9 days after the last tamoxifen treatment), 14, or 18 weeks of age and knee joints were harvested immediately and fixed in 4% paraformaldehyde for 24 hours. Samples were then placed in 10% EDTA in PBS (pH 7.4) for decalcification for 12 days. The EDTA solution was changed every other day. Decalcified limbs were immersed in 30% sucrose in PBS for 24 hours at 4°C. Samples were embedded in the coronal orientation and frozen in Tissue-Tek O.C.T. compound (4583, Sakura Finetek). Frozen sample blocks were cryosectioned serially at 7 μm thickness, and cryosectioning tape (Cryotape type 2C, Section-Lab Co. Ltd.) was used to adhere the sections to the glass slides (*71*).

Each tissue section contained the entire articular cartilage in each compartment of the knee joint. The entire cartilage from all four compartments was assessed by staining with toluidine blue (0.04% toluidine blue in 0.2 M acetate buffer, pH 4.0) or hematoxylin and eosin. Cartilage changes were evaluated using the OARSI grading scale (*72*). Osteophyte size and maturity were assessed on a 0–3 scale as described previously (*73*). Three coronal sections per mouse were taken at 70 μm intervals starting from the middle and moving toward the posterior aspect of the knee joint. The sampling start site was located by referencing landmarks described by Glasson *et al*. (*72*) and was scored by two different scientists blinded to the condition. Mean scores were used in statistical analysis.

For immunohistochemical staining of sections from the middle of the mouse knee joint and human osteoarthritic articular cartilage, tissues underwent antigen retrieval using proteinase K solution (S3020, Dako) for 5 min at room temperature for adseverin, Ihh, and αSMA, tris/EDTA solution (S236784, Dako) for 10 min at 95°C for Ki67, Runx2, and MMP13, and pepsin (2.5 mg/ml) in tris-buffered saline (TBS) (pH 2.0) for 10 min at room temperature for collagen type X. Sections were washed with 0.2% Triton X-100/PBS, blocked with 20% goat serum in 0.2% Triton X-100/PBS, and subsequently incubated overnight at 4°C with primary antibodies for mouse adseverin (1:500; gift from M. Glogauer) (*69*), human adseverin (1:200; ab223055, Abcam), Ihh (1:100; ab39634, Abcam), Ki67 (1:50; ab15580, Abcam), αSMA (1:200; ab5694, Abcam), Runx2 (1:50; NBP1-77461, Novus Biologicals), MMP13 (1:200; 18165-1-AP, Proteintech), and collagen type X (1:1000; ab260040, Abcam). Negative controls consisted of isotype-matched primary antibodies at the same protein concentration. The next day, endogenous peroxidase activity was blocked by incubating slides in 0.3% hydrogen peroxide in PBS for 15 min. After three washes for 5 min each in 0.2% Triton X-100/PBS, sections were incubated in anti-rabbit secondary antibody from MACH 4 Universal HRP-Polymer detection kit (M4U534, Biocare Medical) for 30 min at room temperature. Sections were then washed three times for 5 min each and immunoreactivity was detected using DAB (3,3′-diaminobenzidine) and substrate solution for 1 min, followed by three washes for 5 min with ddH_2O. Slides were then counterstained with hematoxylin (H-3404, Vector Laboratories) and dehydrated, cleared, and mounted as described above. Samples were imaged using an Olympus BX61 microscope and analyzed blinded to the condition using ImageJ software (National Institutes of Health) to quantify immunohistochemically stained positive cells relative to the area of the entire articular cartilage or postnatal growth plate. For the qualitative and quantitative evaluations of histological and immunohistochemical staining, all sections from all biological and technical replicates were stained with one stain/antibody at the same time. This allowed comparison between all conditions to be made to the control sections.

For immunohistochemical staining of in vitro 3D membrane tissues, tissues underwent antigen retrieval using pepsin (2.5 mg/ml) in TBS (pH 2.0) for 10 min at room temperature for collagen type I and II and hyaluronidase (25 mg/ml) in PBS for 30 min at 37°C for aggrecan. Sections were washed with 0.2% Triton X-100/PBS, blocked with 20% goat serum in 0.2% Triton X-100/PBS, and subsequently incubated overnight at 4°C with primary antibodies for aggrecan (1:500; AHP0022, Invitrogen), collagen type I (1:1000; MAB3391, Millipore Sigma), and collagen type II (1:300; MAB8887, Millipore Sigma). Negative controls consisted of replacing the primary antibody with isoform-matched anti-immunoglobulin G (IgG) at the same protein concentration. The next day, tissues were washed with 0.2% Triton X-100/PBS and incubated with Alexa Fluor 594 goat anti-mouse (1:1000; A-11012, Life Technologies) for collagen type I and Alexa Fluor 488 goat anti-mouse (1:1000; A-11008, Life Technologies) for collagen type II and aggrecan at room temperature for 1 hour. Tissues were washed three times, counterstained with 4′,6-diamidino-2-phenylindole (DAPI) (1:1500; Thermo Fisher Scientific) for 10 min, and coverslipped with PermaFluor Mounting Agent (Thermo Fisher Scientific). Samples were imaged using an Olympus IX81 OptiGrid fluorescent microscope.

TUNEL staining was performed on complete cross sections from the middle of the knee joint using the In Situ Cell Death Detection Kit (11684817910, Roche) according to the manufacturer′s protocol. After TUNEL staining, sections were incubated with Alexa Fluor 568 Phalloidin (1:20; A12380, Molecular Probes) to visualize F-actin, and nuclei were stained with DAPI (1:1500; Thermo Fisher Scientific). Samples were imaged using a Quorum spinning disc confocal microscope and analyzed blinded to the condition using ImageJ software (National Institute of Health) to quantify the number of TUNEL-positive articular chondrocytes as a percentage of all cells in the entire articular cartilage or postnatal growth plate.

Cartilage thickness and postnatal growth plate length measurements

For each genotype, the mean of three measurements (locations as indicated in Fig. 2F by red dashed lines) per compartment was determined in three separate sections (same coronal histological slides were used for these evaluations) per mouse and were used to calculate cartilage thickness per compartment (thirty-six measurements per mouse). The same method was used to measure hyaline cartilage thickness in the same location as the total cartilage thickness measurement. Calcified cartilage thickness was calculated by subtracting the hyaline cartilage thickness from the total cartilage thickness.

To assess the postnatal growth plate length, the mean of three measurements at the medial, central, and lateral regions (fig. S9D) was taken from the same three sections used for cartilage thickness

assessments (twenty-seven measurements per mouse). Sections were blinded to the condition and measurements were taken using Image J software (National Institute of Health).

RNA sequencing and analysis

Mice at 10 weeks old were chosen for RNA-seq analysis to determine the effect of adseverin deletion in the absence of OA changes. Articular cartilage was dissected using a scalpel from the femoral condyle and tibial plateau from knee joints of control (n = 3) and knockout (n = 3) mice and collected in RNAlater (R0901, Invitrogen). To increase the yield of RNA extracted, samples were processed with TissueLyser II (Qiagen), and total RNA was isolated using the Qiagen RNeasy kit (74104, Qiagen) according to the manufacturer′s protocol. The quality of sample RNA was accessed by Agilent Fragment Analyzer using High Sensitivity RNA Analysis Kit. Only samples with RNA quality number ≥8.6 were used. A full-length cDNA library was first generated from high-quality total RNA using TaKaRa SMART-Seq v4 Ultra Low Input RNA Kit for Sequencing (634890, TaKaRa) according to the manufacturer′s protocol. The quality and quantity of the purified full-length cDNA were measured by Agilent Fragment Analyzer and Qubit 2.0 (Thermo Fisher Scientific), respectively. The final barcoded sequencing libraries were prepared from full-length cDNA using Illumina Nextera XT Library Prep Kit according to the manufacturer′s protocol. The barcoded cDNA libraries were checked with Agilent Fragment Analyzer for fragment size and quantified with qPCR using Collibri Library Quantification Kit (Thermo Fisher Scientific) on a Bio-Rad CFX96 Touch Real-Time PCR Detection System. Single read with 30 million reads per sample was performed on Illumina NextSeq 500 sequencer for 75 cycles at the Lunenfeld-Tanenbaum Research Institute Sequencing Facility (Toronto, Canada). The quality of RNA-seq raw data was assessed using FastQC (v0.11.9) to ensure high-quality reads (≥35). Reads were aligned to the GRCm38 mouse reference genome using HISAT2 (v2.2.1), and aligned reads were counted using featureCounts (v2.0.1). Normalization and analysis of DEGs were done in R (v4.0.5) using the DESeq2 (v1.30.1) package. The resulting P values were adjusted for false discovery rate (FDR) using the Benjamini-Hochber method. The threshold for significant DEGs was FDR < 0.1 and $|\log_2 \text{fold change}| \geq 0.2$. Gene set enrichment analysis was done on DEGs using the hallmark, REACTOME, Kyoto Encyclopedia of Genes and Genomes, and Gene Ontology gene sets in the Molecular Signatures Database (MSigDB).

Atomic force microscopy

Knee joint from 10-week-old control and knockout mice was harvested, embedded in Tissue-Tek O.C.T. compound (4583, Sakura Finetek), and immediately frozen. Frozen sample blocks were cryosectioned serially at 30 μm thickness and cryosectioning tape (Cryotape type 2C, Section-Lab Co. Ltd.) was used to stabilize and adhere the sections to the glass slides (*71*). Sections were kept at −20°C until use.

IT-AFM was performed using a Zeiss Axiovert 200M microscope equipped with NanoWizard 4 (JPK Instruments). For nanoscale force curve measurements, silicon nitride MLCT-BIO E cantilevers (Bruker) containing quadratic pyramid tips with a nominal radius of 20 nm and spring constant of 0.1 N/m were used. Because of the biological properties of articular cartilage, all force curve measurements were done in pH 7.4 PBS supplemented with protease inhibitor (Roche). The spring constant and sensitivity of the cantilevers were calibrated and determined using the thermal noise method (*74*). The mean spring constant of three repeated calibrations was used for data analysis. Force curve mapping with an area of 3 × 3 μm consisting of 16 × 16 individual force curves was measured for each articular cartilage zones (superficial, middle, and deep). For each genotype, three animals were analyzed, and two serial tissue sections (30 μm interval) were obtained per animal starting from the middle of the knee. The midpoint of the MTP cartilage (as determined by measuring the width of the entire compartment) was scanned in each cartilage zone (depicted in Fig. 3I), yielding a total of 1536 force curves per animal. Data analysis was done blinded to the condition using JPK Data Processing Software (v6.3.5) and Young′s modulus (E) was determined from the retract portion of the force curves using a modified Hertz model for quadratic pyramid indenter.

Primary culture of murine articular chondrocytes

For murine cultures, articular chondrocyte isolation was adapted from a published protocol (*75*). Briefly, control and knockout mice were euthanized at 10 weeks of age. Under a dissection microscope, articular cartilage was dissected with a scalpel from the femoral condyle and tibial plateau from the knees and collected in sterile cold PBS supplemented with 1% antimycotic/biotic. Tissues were washed with vigorous shaking three times in cold PBS followed by digestion in collagenase A (3 mg/ml; Roche Diagnostics, Germany) for 45 min at 37°C. Cartilage pieces were retrieved with sterile forceps and placed into a new petri dish with collagenase A (0.5 mg/ml) and digested for 16 to 18 hours at 37°C. The next day, cartilage pieces were pipetted up and down to ensure the full release of cells, and then filtered sequentially with a 100 and 40 μm cell strainer. Chondrocytes were then washed with Dulbecco′s modified Eagle′s medium (DMEM) (319-010-CL, Wisent) supplemented with 10% FBS, pelleted, and resuspended for counting. Each biological replicate was obtained from pooling cartilage pieces from three independent mice to obtain sufficient cell numbers for an experiment. Cells were seeded in monolayer or 3D membrane cultures depending on the experimental conditions.

Immunocytochemistry

Immunocytochemistry was performed as previously described with slight modifications (*13*). Primary mouse articular chondrocytes from 10-week-old control and knockout mice were seeded at a density of 3.5×10^4 cells/cm^2 on glass coverslips. At 3 and 7 days of monolayer culture, cells were washed with PBS and fixed in 4% paraformaldehyde at room temperature for 10 min. Cells were washed with 0.2% Triton X-100/PBS, blocked in 10% goat serum in 0.2% Triton X-100/PBS, and then incubated overnight at 4°C with adseverin antibody (1:500; gift from M. Glogauer) (*69*). Samples were washed and incubated with Alexa Fluor 488 (1:1000; A-11008, Life Technologies) and Alexa Fluor 568 Phalloidin (1:20; A12380, Molecular Probes) to visualize F-actin. Nuclei were stained with DAPI (1:1500; Thermo Fisher Scientific). Negative controls consisted of replacing the primary antibody with isoform-matched anti-IgG at the same protein concentration. Coverslips were washed with PBS and mounted on glass slides using PermaFluor Mounting Agent (ThermoFisher Scientific). Images were taken using a Quorum spinning disc confocal microscope.

Protein extraction and Western blot analysis

Primary bovine articular chondrocytes seeded in monolayer at 5×10^4 cells/cm^2 were treated with IL-1β for up to 7 days and harvested for protein every 24 hours. For murine cultures, primary articular chondrocytes were harvested after 72 hours of monolayer culture after initial seeding at 4.2×10^4 cells/cm^2. Total protein extraction with radioimmunoprecipitation assay (RIPA) buffer and Western blot analysis was done as previously described (*13*). For Western blot analysis, primary antibodies for bovine adseverin (1:2000; ab96105, Abcam), mouse adseverin (1:10,000; gift from M. Glogauer) (*69*), and pan-actin (1:1000; MAB1501, Millipore Sigma) were used. For the loading control, glyceraldehyde-3-phosphate dehydrogenase (1:2000; ABS16, Millipore Sigma) was used. Immunoreactivity was detected using Amersham ECL Prime Western Blotting Detection Reagent kit (RPN2236, GE Healthcare) and quantified using densitometry via ImageJ software (National Institutes of Health).

G-/F-actin quantification

Mouse primary articular chondrocytes were harvested after 72 hours of monolayer culture after initial seeding at 4.2×10^4 cells/cm^2. G-/F-actin was measured using the differential Triton X-100 solubility method as previously described (*13*). Briefly, cells were scraped in PBS and pelleted. Pellets were resuspended in 250 μl of 0.1% Triton X-100 in PBS with cOmplete Mini protease inhibitor (Roche) and agitated on a rocker for 5 min. The resuspended cells were centrifuged at 14,000*g* at 4°C for 5 min. The supernatant was collected as the globular actin. The remaining pellet consisting predominately of filamentous actin was resuspended in 250 μl of RIPA buffer for 30 min at 4°C with agitation on a rocker. Forty microliters of globular and filamentous actin fractions was mixed with Laemmli buffer, separated by electrophoresis on 10% polyacrylamide gels, and then analyzed by Western blot using pan-actin (1:1000; MAB1501, Millipore Sigma) antibody. Immunoreactivity was detected using Amersham ECL Prime Western Blotting Detection Reagent kit (RPN2236, GE Healthcare) and quantified using densitometry via ImageJ software (National Institutes of Health).

In vitro mineralization

The primary control and knockout murine articular chondrocytes were seeded at 1.8×10^5 cells/cm^2 in a 96-well plate and cultured in DMEM supplemented with 10% FBS for 3 days. The next day, the media were changed to DMEM supplemented with 10% FBS and ascorbic acid (100 μg/ml) for 4 days to allow tissue formation. To induce mineralization, cells were then cultured in DMEM with 10% FBS, ascorbic acid (100 μg/ml), and 1 mM inorganic phosphate for 3 days. The culture medium was refreshed every other day. Calcium deposits were visualized using Von Kossa staining. Briefly, cells were fixed in 4% paraformaldehyde for 10 min, washed with ddH_2O for 5 min, and incubated for 15 min under ultraviolet light with 5% (w/v) silver nitrate solution. Then, cells were washed with ddH_2O and followed by 1% (w/v) sodium thiosulfate for 5 min and lastly washed with ddH_2O for 5 min before imaging on a Leica DM IL microscope.

In vitro 3D membrane cultures

Before use, membrane inserts (3381, Corning) were coated with 50 μl of collagen type II (C9301, Sigma-Aldrich) solution (0.05 mg/ml dissolved in 0.01% acetic acid) and dried overnight under sterile conditions. Membranes were washed with PBS immediately before use. Murine articular chondrocytes were seeded onto membranes at 5.3×10^6 cells/cm^2 in DMEM supplemented with 10% FBS. On day 4, ascorbic acid (100 μg/ml) was added to the media and cultured for 2 weeks. The culture medium was changed every other day.

Biochemical tissue content

In vitro formed murine cartilage tissues were digested with papain (40 μg/ml; Sigma-Aldrich) in buffer containing 20 mM ammonium acetate, 1 mM EDTA, and 2 mmol dithiothreitol at pH 6.2 for 48 hours at 65°C. DNA content was quantified by the Hoechst 33258 fluorometric assay (excitation λ = 356 nm, emission λ = 458 nm) (*76*). The DNA standard curve was generated using calf thymus DNA (Sigma-Aldrich). The sulfated glycosaminoglycan content of the tissue was quantified using the dimethylmethylene blue assay (λ = 525 nm) (*76*). Chondroitin sulfate (Sigma-Aldrich) was used to generate the standard curve.

Human osteoarthritic articular cartilage

Human femoral condyles resected during arthroplasty surgery for OA were obtained with informed patient consent and Research Ethics Board approval (REB; #05-0071E, Mount Sinai Hospital). Full-thickness articular cartilage was taken from macroscopically intact areas, fixed in 4% paraformaldehyde for 24 hours, and dehydrated with 30% sucrose in PBS for 24 hours at 4°C. Samples were frozen in Tissue-Tek O.C.T. compound (4583, Sakura Finetek). Frozen sample blocks were cryosectioned serially at 7 μm thickness and fixed to the slide using cryosectioning tape (Cryotape type 2C, Section-Lab Co. Ltd.) (*71*).

Statistical analysis

At least three experiments were performed using independent biological replicates for studies involving in vitro grown cells. The number of mice used is indicated in the figures. Statistical analysis was done using the Student's unpaired two-tailed *t* test for comparisons between two groups and one-way analysis of variance (ANOVA) followed by Dunnett's post hoc test for more than two groups. Results are expressed as means ± SEM, median, and interquartile range box plots, or dot plots; whiskers are plotted using the Tukey method. Statistical significance was assigned at $P < 0.05$ and *P* values are indicated in the figures. All statistical analyses were performed using GraphPad Prism (v7.0).

Supplementary Materials

This PDF file includes:

Figs. S1 to S15
Table S1
Legend for data S1

Other Supplementary Material for this manuscript includes the following:

Data S1

REFERENCES AND NOTES

1. P. Singh, K. B. Marcu, M. B. Goldring, M. Otero, Phenotypic instability of chondrocytes in osteoarthritis: On a path to hypertrophy. *Ann. N. Y. Acad. Sci.* **1442**, 17–34 (2019).

2. E. Charlier, C. Deroyer, F. Ciregia, O. Malaise, S. Neuville, Z. Plener, M. Malaise, D. de Seny, Chondrocyte dedifferentiation and osteoarthritis (OA). *Biochem. Pharmacol.* **165**, 49–65 (2019).
3. M. J. López-Armada, B. Caramés, M. Lires-Deán, B. Cillero-Pastor, C. Ruiz-Romero, F. Galdo, F. J. Blanco, Cytokines, tumor necrosis factor-α and interleukin-1β, differentially regulate apoptosis in osteoarthritis cultured human chondrocytes. *Osteoarthr. Cartil.* **14**, 660–669 (2006).
4. H. S. Hwang, H. A. Kim, Chondrocyte apoptosis in the pathogenesis of osteoarthritis. *Int. J. Mol. Sci.* **16**, 26035–26054 (2015).
5. C. Povýšil, R. Kaňa, P. Dundr, D. Tvrdík, M. Horák, J. Vaculík, A. Podškubka, R. Kubeš, Distribution of chondrocytes containing alpha-smooth muscle actin in human normal, osteoarthrotic, and transplanted articular cartilage. *Pathol. Res. Pract.* **204**, 883–890 (2008).
6. A. A. Pitsillides, F. Beier, Cartilage biology in osteoarthritis—Lessons from developmental biology. *Nat. Rev. Rheumatol.* **7**, 654–663 (2011).
7. E. G. J. Ripmeester, U. T. Timur, M. M. J. Caron, T. J. M. Welting, Recent insights into the contribution of the changing hypertrophic chondrocyte phenotype in the development and progression of osteoarthritis. *Front. Bioeng. Biotechnol.* **6**, 18 (2018).
8. J. C. Lauer, M. Selig, M. L. Hart, B. Kurz, B. Rolauffs, Articular chondrocyte phenotype regulation through the cytoskeleton and the signaling processes that originate from or converge on the cytoskeleton: Towards a novel understanding of the intersection between actin dynamics and chondrogenic function. *Int. J. Mol. Sci.* **22**, 3279 (2021).
9. A. Woods, G. Wang, F. Beier, Regulation of chondrocyte differentiation by the actin cytoskeleton and adhesive interactions. *J. Cell. Physiol.* **213**, 1–8 (2007).
10. P. D. Brown, P. D. Benya, Alterations in chondrocyte cytoskeletal architecture during phenotypic modulation by retinoic acid and dihydrocytochalasin B-induced reexpression. *J. Cell Biol.* **106**, 171–179 (1988).
11. M. D. Gardiner, T. L. Vincent, C. Driscoll, A. Burleigh, G. Bou-Gharios, J. Saklatvala, H. Nagase, A. Chanalaris, Transcriptional analysis of micro-dissected articular cartilage in post-traumatic murine osteoarthritis. *Osteoarthr. Cartil.* **23**, 616–628 (2015).
12. R. Rollín, P. Tornero, F. Marco, E. Camafeita, E. Calvo, L. López-Durán, J. Á. Jover, J. A. López, J. R. Lamas, B. Fernández-Gutiérrez, Differential proteome of articular chondrocytes from patients with osteoarthritis. *J. Proteomics Bioinform.* **01**, 267–280 (2008).
13. B. Chan, J. Parreno, M. Glogauer, Y. Wang, R. Kandel, Adseverin, an actin binding protein, regulates articular chondrocyte phenotype. *J. Tissue Eng. Regen. Med.* **13**, 1438–1452 (2019).
14. J. C. Fernandes, J. Martel-Pelletier, J. P. Pelletier, The role of cytokines in osteoarthritis pathophysiology. *Biorheology* **39**, 237–246 (2002).
15. Z. Jenei-Lanzl, A. Meurer, F. Zaucke, Interleukin-1β signaling in osteoarthritis–chondrocytes in focus. *Cell. Signal.* **53**, 212–223 (2019).
16. S. Hashimoto, R. L. Ochs, S. Komiya, M. Lotz, Linkage of chondrocyte apoptosis and cartilage degradation in human osteoarthritis. *Arthritis Rheum.* **41**, 1632–1638 (1998).
17. D. Mistry, Y. Oue, M. G. Chambers, M. V. Kayser, R. M. Mason, Chondrocyte death during murine osteoarthritis. *Osteoarthr. Cartil.* **12**, 131–141 (2004).
18. P. Alberton, H. C. Dugonitsch, B. Hartmann, P. Li, Z. Farkas, M. M. Saller, H. Clausen-Schaumann, A. Aszodi, Aggrecan hypomorphism compromises articular cartilage biomechanical properties and is associated with increased incidence of spontaneous osteoarthritis. *Int. J. Mol. Sci.* **20**, 1008 (2019).
19. B. Doyran, W. Tong, Q. Li, H. Jia, X. Zhang, C. Chen, M. Enomoto-Iwamoto, X. L. Lu, L. Qin, L. Han, Nanoindentation modulus of murine cartilage: A sensitive indicator of the initiation and progression of post-traumatic osteoarthritis. *Osteoarthr. Cartil.* **25**, 108–117 (2017).
20. M. Stolz, R. Gottardi, R. Raiteri, S. Miot, I. Martin, R. Imer, U. Staufer, A. Raducanu, M. Düggelin, W. Baschong, A. U. Daniels, N. F. Friederich, A. Aszodi, U. Aebi, Early detection of aging cartilage and osteoarthritis in mice and patient samples using atomic force microscopy. *Nat. Nanotechnol.* **4**, 186–192 (2009).
21. Y. Maeda, E. Nakamura, M. T. Nguyen, L. J. Suva, F. L. Swain, M. S. Razzaque, S. Mackem, B. Lanske, Indian hedgehog produced by postnatal chondrocytes is essential for maintaining a growth plate and trabecular bone. *Proc. Natl. Acad. Sci. U.S.A.* **104**, 6382–6387 (2007).
22. J. Yang, P. Andre, L. Ye, Y. Z. Yang, The hedgehog signalling pathway in bone formation. *Int. J. Oral Sci.* **7**, 73–79 (2015).
23. B. St-Jacques, M. Hammerschmidt, A. P. McMahon, Indian hedgehog signaling regulates proliferation and differentiation of chondrocytes and is essential for bone formation. *Genes Dev.* **13**, 2072–2086 (1999).
24. J. Martel-Pelletier, Pathophysiology of osteoarthritis. *Osteoarthr. Cartil.* **12**, 31–33 (2004).
25. J. Martel-Pelletier, A. J. Barr, F. M. Cicuttini, P. G. Conaghan, C. Cooper, M. B. Goldring, S. R. Goldring, G. Jones, A. J. Teichtahl, J. P. Pelletier, Osteoarthritis. *Nat. Rev. Dis. Prim.* **2**, 16072 (2016).
26. S. S. Glasson, T. J. Blanchet, E. A. Morris, The surgical destabilization of the medial meniscus (DMM) model of osteoarthritis in the 129/SvEv mouse. *Osteoarthr. Cartil.* **15**, 1061–1069 (2007).
27. H. L. Ma, T. J. Blanchet, D. Peluso, B. Hopkins, E. A. Morris, S. S. Glasson, Osteoarthritis severity is sex dependent in a surgical mouse model. *Osteoarthr. Cartil.* **15**, 695–700 (2007).
28. A. M. Ruiz-Zapata, A. Heinz, M. H. Kerkhof, C. van de Westerlo-Van Rijt, C. E. H. Schmelzer, R. Stoop, K. B. Kluivers, E. Oosterwijk, Extracellular matrix stiffness and composition regulate the myofibroblast differentiation of vaginal fibroblasts. *Int. J. Mol. Sci.* **21**, 1–15 (2020).
29. R. G. Wells, D. E. Discher, Matrix elasticity, cytoskeletal tension, and TGF-β: The insoluble and soluble meet. *Sci. Signal.* **1**, pe13 (2008).
30. A. Fioravanti, F. Nerucci, M. Annefeld, G. Collodel, R. Marcolongo, Morphological and cytoskeletal aspects of cultivated normal and osteoarthritic human articular chondrocytes after cyclical pressure: A pilot study. *Clin. Exp. Rheumatol.* **21**, 739–746 (2003).
31. N. Capín-Gutiérrez, P. Talamás-Rohana, A. González-Robles, C. Lavalle-Montalvo, J. B. Kourí, Cytoskeleton disruption in chondrocytes from a rat osteoarthrosic (OA)-induced model: Its potential role in OA pathogenesis. *Histol. Histopathol.* **19**, 1125–1132 (2004).
32. N. A. Pascarelli, G. Collodel, E. Moretti, S. Cheleschi, A. Fioravanti, Changes in ultrastructure and cytoskeletal aspects of human normal and osteoarthritic chondrocytes exposed to interleukin-1β and cyclical hydrostatic pressure. *Int. J. Mol. Sci.* **16**, 26019–26034 (2015).
33. W. Lee, R. J. Nims, A. Savadipour, Q. Zhang, H. A. Leddy, F. Liu, A. L. McNulty, Y. Chen, F. Guilak, W. B. Liedtke, Inflammatory signaling sensitizes Piezo1 mechanotransduction in articular chondrocytes as a pathogenic feed-forward mechanism in osteoarthritis. *Proc. Natl. Acad. Sci. U.S.A.* **118**, e2001611118 (2021).
34. P. Lorenzo, M. T. Bayliss, D. Heinegård, Altered patterns and synthesis of extracellular matrix macromolecules in early osteoarthritis. *Matrix Biol.* **23**, 381–391 (2004).
35. D. R. Haudenschild, J. Chen, N. Steklov, M. K. Lotz, D. D. D'Lima, Characterization of the chondrocyte actin cytoskeleton in living three-dimensional culture: Response to anabolic and catabolic stimuli. *MCB Mol. Cell. Biomech.* **6**, 135–144 (2009).
36. A. Holzinger, Jasplakinolide: An actin-specific reagent that promotes actin polymerization. *Methods Mol. Biol.* **586**, 71–87 (2009).
37. C. Odaka, M. L. Sanders, P. Crews, Jasplakinolide induces apoptosis in various transformed cell lines by a caspase-3-like protease-dependent pathway. *Clin. Diagn. Lab. Immunol.* **7**, 947–952 (2000).
38. J. Y. Rao, Y. S. Jin, Q. L. Zheng, J. Cheng, J. Tai, G. P. Hemstreet, Alterations of the actin polymerization status as an apoptotic morphological effector in HL-60 cells. *J. Cell. Biochem.* **75**, 686–697 (1999).
39. M. C. Peitsch, B. Polzar, H. Stephan, T. Crompton, H. R. MacDonald, H. G. Mannherz, J. Tschopp, Characterization of the endogenous deoxyribonuclease involved in nuclear DNA degradation during apoptosis (programmed cell death). *EMBO J.* **12**, 371–377 (1993).
40. D. Chhabra, S. Bao, C. G. Dos Remedios, The distribution of cofilin and DNase I in vivo. *Cell Res.* **12**, 207–214 (2002).
41. X. Xu, J. G. Forbes, M. Colombini, Actin modulates the gating of Neurospora crassa VDAC. *J. Membr. Biol.* **180**, 73–81 (2001).
42. J. D. Ly, D. R. Grubb, A. Lawen, The mitochondrial membrane potential (δψm) in apoptosis; an update. *Apoptosis* **8**, 115–128 (2003).
43. M. Desouza, P. W. Gunning, J. R. Stehn, The actin cytoskeleton as a sensor and mediator of apoptosis. *Bioarchitecture.* **2**, 75–87 (2012).
44. R. C. Koya, H. Fujita, S. Shimizu, M. Ohtsu, M. Takimoto, Y. Tsujimoto, N. Kuzumaki, Gelsolin inhibits apoptosis by blocking mitochondrial membrane potential loss and cytochrome c release. *J. Biol. Chem.* **275**, 15343–15349 (2000).
45. H. Kusano, S. Shimizu, R. C. Koya, H. Fujita, S. Kamada, N. Kuzumaki, Y. Tsujimoto, Human gelsolin prevents apoptosis by inhibiting apoptotic mitochondrial changes via closing VDAC. *Oncogene* **19**, 4807–4814 (2000).
46. U. Ghoshdastider, D. Popp, L. D. Burtnick, R. C. Robinson, The expanding superfamily of gelsolin homology domain proteins. *Cytoskeleton* **70**, 775–795 (2013).
47. V. Shoshan-Barmatz, M. Zakar, K. Rosenthal, S. Abu-Hamad, Key regions of VDAC1 functioning in apoptosis induction and regulation by hexokinase. *Biochim. Biophys. Acta - Bioenerg.* **1787**, 421–430 (2009).
48. Q. Q. Wu, Y. Zhang, Q. Chen, Indian hedgehog is an essential component of mechanotransduction complex to stimulate chondrocyte proliferation. *J. Biol. Chem.* **276**, 35290–35296 (2001).
49. P. M. Van der Kraan, W. B. Van den Berg, Chondrocyte hypertrophy and osteoarthritis: Role in initiation and progression of cartilage degeneration? *Osteoarthr. Cartil.* **20**, 223–232 (2012).
50. F. Wei, J. Zhou, X. Wei, J. Zhang, B. C. Fleming, R. Terek, M. Pei, Q. Chen, T. Liu, L. Wei, Activation of Indian hedgehog promotes chondrocyte hypertrophy and upregulation of MMP-13 in human osteoarthritic cartilage. *Osteoarthr. Cartil.* **20**, 755–763 (2012).

51. A. C. Lin, B. L. Seeto, J. M. Bartoszko, M. A. Khoury, H. Whetstone, L. Ho, C. Hsu, A. S. Ali, B. A. Alman, Modulating hedgehog signaling can attenuate the severity of osteoarthritis. *Nat. Med.* **15**, 1421–1425 (2009).
52. J. Zhou, Q. Chen, B. Lanske, B. C. Fleming, R. Terek, X. Wei, G. Zhang, S. Wang, K. Li, L. Wei, Disrupting the Indian hedgehog signaling pathway in vivo attenuates surgically induced osteoarthritis progression in Col2a1-CreERT2; Ihhfl/fl mice. *Arthritis Res. Ther.* **16**, R11 (2014).
53. L. Izzi, M. Lévesque, S. Morin, D. Laniel, B. C. Wilkes, F. Mille, R. S. Krauss, A. P. McMahon, B. L. Allen, F. Charron, Boc and gas1 each form distinct shh receptor complexes with ptch1 and are required for shh-mediated cell proliferation. *Dev. Cell* **20**, 788–801 (2011).
54. B. L. Allen, T. Tenzen, A. P. McMahon, The hedgehog-binding proteins Gas1 and Cdo co-operate to positively regulate Shh signaling during mouse development. *Genes Dev.* **21**, 1244–1257 (2007).
55. D. C. Martinelli, C. M. Fan, Gas1 extends the range of hedgehog action by facilitating its signaling. *Genes Dev.* **21**, 1231–1243 (2007).
56. D. Nurminsky, C. Magee, L. Faverman, M. Nurminskaya, Regulation of chondrocyte differentiation by actin-severing protein adseverin. *Dev. Biol.* **302**, 427–437 (2007).
57. E. J. Blain, Involvement of the cytoskeletal elements in articular cartilage homeostasis and pathology. *Int. J. Exp. Pathol.* **90**, 1–15 (2009).
58. M. L. Drummond, M. Li, E. Tarapore, T. T. L. Nguyen, B. J. Barouni, S. Cruz, K. C. Tan, A. E. Oro, S. X. Atwood, Actin polymerization controls cilia-mediated signaling. *J. Cell Biol.* **217**, 3255–3266 (2018).
59. Z. Zhao, Y. Li, M. Wang, S. Zhao, Z. Zhao, J. Fang, Mechanotransduction pathways in the regulation of cartilage chondrocyte homoeostasis. *J. Cell. Mol. Med.* **24**, 5408–5419 (2020).
60. K. K. Mak, H. M. Kronenberg, P. T. Chuang, S. Mackem, Y. Yang, Indian hedgehog signals independently of PTHrP to promote chondrocyte hypertrophy. *Development* **135**, 1947–1956 (2008).
61. T. L. Vincent, A. K. T. Wann, Mechanoadaptation: Articular cartilage through thick and thin. *J. Physiol.* **597**, 1271–1281 (2019).
62. C. R. Coveney, L. Zhu, J. Miotla-Zarebska, B. Stott, I. Parisi, V. Batchelor, C. Duarte, E. Chang, E. McSorley, T. L. Vincent, A. K. T. Wann, Role of ciliary protein intraflagellar transport protein 88 in the regulation of cartilage thickness and osteoarthritis development in mice. *Arthritis Rheumatol.* **74**, 49–59 (2022).
63. Y. Gao, S. Liu, J. Huang, W. Guo, J. Chen, L. Zhang, B. Zhao, J. Peng, A. Wang, Y. Wang, W. Xu, S. Lu, M. Yuan, Q. Guo, The ECM-cell interaction of cartilage extracellular matrix on chondrocytes. *Biomed. Res. Int.* **2014**, 1–8 (2014).
64. S. M. Frisch, R. A. Screaton, Anoikis mechanisms. *Curr. Opin. Cell Biol.* **13**, 555–562 (2001).
65. M. Rikkers, J. V. Korpershoek, R. Levato, J. Malda, L. A. Vonk, The clinical potential of articular cartilage-derived progenitor cells: A systematic review. *NPJ Regen. Med.* **7**, 2 (2022).
66. P. M. van der Kraan, W. B. van den Berg, Osteophytes: Relevance and biology. *Osteoarthr. Cartil.* **15**, 237–244 (2007).
67. D. Seol, D. J. McCabe, H. Choe, H. Zheng, Y. Yu, K. Jang, M. W. Walter, A. D. Lehman, L. Ding, J. A. Buckwalter, J. A. Martin, Chondrogenic progenitor cells respond to cartilage injury. *Arthritis Rheum.* **64**, 3626–3637 (2012).
68. T. Wöllert, G. M. Langford, Super-resolution imaging of the actin cytoskeleton in living cells using TIRF-SIM. *Methods Mol. Biol.* **2364**, 3–24 (2022).
69. H. Jiang, Y. Wang, A. Viniegra, C. Sima, C. A. McCulloch, M. Glogauer, Adseverin plays a role in osteoclast differentiation and periodontal disease-mediated bone loss. *FASEB J.* **29**, 2281–2291 (2015).
70. S. P. Henry, C. W. Jang, J. M. Deng, Z. Zhang, R. R. Behringer, B. De Crombrugghe, Generation of aggrecan-CreERT2 knockin mice for inducible Cre activity in adult cartilage. *Genesis* **47**, 805–814 (2009).
71. N. A. Dyment, X. Jiang, L. Chen, S. H. Hong, D. J. Adams, C. Ackert-Bicknell, D. G. Shin, D. W. Rowe, High-throughput, multi-image cryohistology of mineralized tissues. *J. Vis. Exp.*, 54468 (2016).
72. S. S. Glasson, M. G. Chambers, W. B. Van Den Berg, C. B. Little, The OARSI histopathology initiative–recommendations for histological assessments of osteoarthritis in the mouse. *Osteoarthr. Cartil.* **18**, S17–S23 (2010).
73. C. B. Little, A. Barai, D. Burkhardt, S. M. Smith, A. J. Fosang, Z. Werb, M. Shah, E. W. Thompson, Matrix metalloproteinase 13-deficient mice are resistant to osteoarthritic cartilage erosion but not chondrocyte hypertrophy or osteophyte development. *Arthritis Rheum.* **60**, 3723–3733 (2009).
74. H. J. Butt, M. Jaschke, Calculation of thermal noise in atomic force microscopy. *Nanotechnology* **6**, 1–7 (1995).
75. M. Gosset, F. Berenbaum, S. Thirion, C. Jacques, Primary culture and phenotyping of murine chondrocytes. *Nat. Protoc.* **3**, 1253–1260 (2008).
76. S. D. Waldman, M. D. Grynpas, R. M. Pilliar, R. A. Kandel, Characterization of cartilagenous tissue formed on calcium polyphosphate substrates in vitro. *J. Biomed. Mater. Res.* **62**, 323–330 (2002).

Acknowledgments: We thank the veterinary and surgical staff at the Division of Comparative Medicine, University of Toronto, for assistance throughout the surgical procedures and for maintaining the welfare of the animals used in this study. We also thank R. Bielecki for microscopy expertise. **Funding:** This work was supported by NSERC Discovery Grant RGPIN-2016-06088 (to R.K.), University of Toronto Fellowship (to B.C.), Ontario Student Opportunity Trust Funds Award (to B.C.), Queen Elizabeth II Graduate Scholarship in Science & Technology (to B.C.), Ontario Graduate Scholarship (to B.C.). **Author contributions:** Conceptualization: B.C. and R.K. Methodology: B.C., F.B., S.B., M.G., Y.W., B.H. Software: B.C., J.W., and K.C. Formal analysis: B.C. and R.K. Investigation: B.C. and R.K. Resources: R.K., M.G., Y.W., B.H., J.W., K.C., J.P., and S.A. Visualization: B.C. Supervision: R.K. Funding acquisition: R.K. Writing—original draft: B.C. and R.K. Writing—review and editing: All authors. **Competing interests:** The authors declare that they have no competing interests. **Data and materials availability:** All data needed to evaluate the conclusions in the paper are present in the paper and/or the Supplementary Materials. Raw RNA sequencing data have been deposited to the NCBI GEO under accession code (GSE209578). RNA sequence mapping used GRCm38 *M. musculus* genome (www.ncbi.nlm.nih.gov/assembly/GCF_000001635.20). The following figures have associated source data: Figs. 1 (A to D, G, I, and K), 2 (G to I and K), 3 (E, G, and J to L), 4 (B to D and F to H), 5 (B, D, F, I, and K), 6 (B, D, F, I, and K), 7 (C to E), 8F, and 9 (C, E, G, I, K, and M) and figs. S2 (B, D, and F), S7 (B and D), S8 (G and H), S9 (E to J), S10 (B and E), S11C, S12C, S13 (C and F), and S14 (C and E).

Submitted 12 October 2022
Accepted 6 July 2023
Published 4 August 2023
10.1126/sciadv.adf1130